Article

Cell

A Genome-wide CRISPR Screen in *Toxoplasma* Identifies Essential Apicomplexan Genes

Graphical Abstract

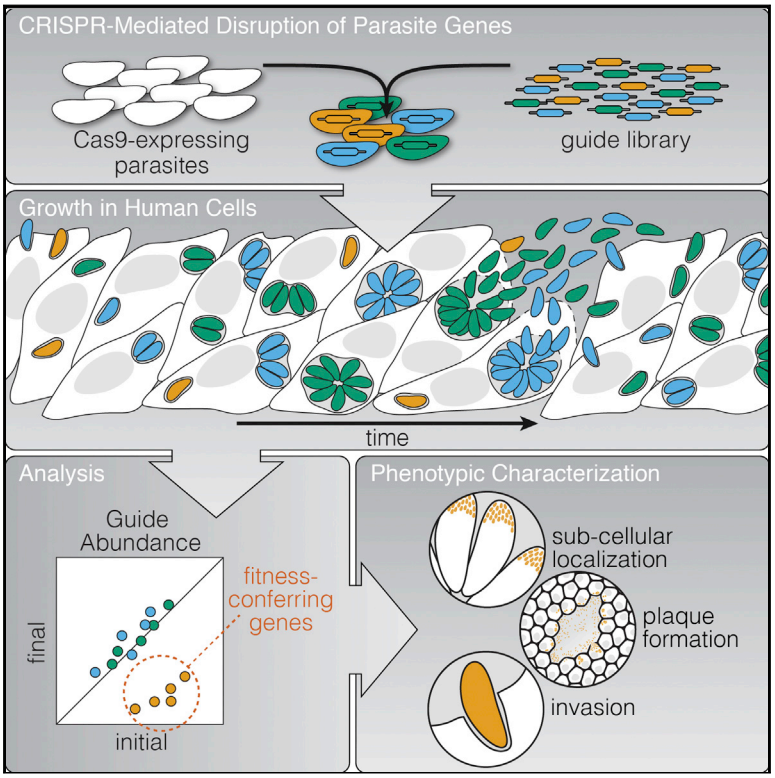

Authors

Saima M. Sidik, Diego Huet, Suresh M. Ganesan, ..., Vern B. Carruthers, Jacquin C. Niles, Sebastian Lourido

Correspondence

lourido@wi.mit.edu

In Brief

The first genome-wide genetic screen of an apicomplexan parasite identifies an invasion factor essential for the fitness of all parasites in this phylum, including those causing malaria and toxoplasmosis.

Highlights

- CRISPR enables the first genome-wide loss-of-function screen in *T. gondii*
- The screen measures each gene's impact during infection of human fibroblasts
- Functional assays validate the essentiality of formerly uncharacterized proteins
- An invasion factor found in all apicomplexans is essential in malarial parasites

Sidik et al., 2016, Cell *167*, 1423–1435
September 8, 2016
http://dx.doi.org/10.1016/j.cell.2016.08.019

CellPress

Cell

A Genome-wide CRISPR Screen in *Toxoplasma* Identifies Essential Apicomplexan Genes

Saima M. Sidik,[1,7] Diego Huet,[1,7] Suresh M. Ganesan,[2] My-Hang Huynh,[3] Tim Wang,[1,4,5] Armiyaw S. Nasamu,[2] Prathapan Thiru,[1] Jeroen P.J. Saeij,[6] Vern B. Carruthers,[3] Jacquin C. Niles,[2] and Sebastian Lourido[1,8,*]
[1]Whitehead Institute for Biomedical Research, Cambridge, MA 02142, USA
[2]Department of Biological Engineering, Massachusetts Institute of Technology, Cambridge, MA 02139, USA
[3]Department of Microbiology and Immunology, University of Michigan School of Medicine, Ann Arbor, MI 48109, USA
[4]Department of Biology, Massachusetts Institute of Technology, Cambridge, MA 02139 USA
[5]Broad Institute of MIT and Harvard, Cambridge, MA 02142, USA
[6]Department of Pathology, Microbiology and Immunology, University of California, Davis, Davis, CA 95616, USA
[7]Co-first author
[8]Lead Contact
*Correspondence: lourido@wi.mit.edu
http://dx.doi.org/10.1016/j.cell.2016.08.019

SUMMARY

Apicomplexan parasites are leading causes of human and livestock diseases such as malaria and toxoplasmosis, yet most of their genes remain uncharacterized. Here, we present the first genome-wide genetic screen of an apicomplexan. We adapted CRISPR/Cas9 to assess the contribution of each gene from the parasite *Toxoplasma gondii* during infection of human fibroblasts. Our analysis defines ~200 previously uncharacterized, fitness-conferring genes unique to the phylum, from which 16 were investigated, revealing essential functions during infection of human cells. Secondary screens identify as an invasion factor the claudin-like apicomplexan microneme protein (CLAMP), which resembles mammalian tight-junction proteins and localizes to secretory organelles, making it critical to the initiation of infection. CLAMP is present throughout sequenced apicomplexan genomes and is essential during the asexual stages of the malaria parasite *Plasmodium falciparum*. These results provide broad-based functional information on *T. gondii* genes and will facilitate future approaches to expand the horizon of antiparasitic interventions.

INTRODUCTION

Apicomplexans comprise a phylum of over 5,000 obligate parasites whose hosts span the animal kingdom (Levine, 1988). Several species are leading causes of infant mortality, such as *Plasmodium* and *Cryptosporidium* spp., which cause malaria and severe diarrhea, respectively (Checkley et al., 2015; World Health Organization, 2014). *Toxoplasma gondii*, predicted to establish lifelong infections in a quarter of the world's population, can cause life-threatening disease in immune-compromised individuals or when contracted congenitally (Pappas et al., 2009). Despite their importance to global health, apicomplexans remain enigmatic. Only a handful of species have been studied, and fewer than half of their genes have been functionally annotated. The ease with which *T. gondii* can be cultured, along with the genetic tractability that comes with its balanced nucleotide composition and high transfection rates, presents compelling arguments for using this parasite as a model apicomplexan. Scalable methods to assess gene function in *T. gondii* could therefore greatly extend our understanding of apicomplexan biology.

Genetic crosses have long been used to identify loci responsible for phenotypes ranging from drug resistance in *Plasmodium falciparum* (Wellems et al., 1991) to virulence in *T. gondii* (Saeij et al., 2006; Taylor et al., 2006). However, completing the sexual cycles of *T. gondii* or *Plasmodium* spp. in cats or mosquitoes is challenging, and the traits examined must vary within the species. Spontaneous mutations, or those induced chemically or by transposition, can sample a wider range of phenotypes (Crabb et al., 2011; Farrell et al., 2014; Flannery et al., 2013), but the population size required to achieve saturation is impractical, and causal mutations are often difficult to identify.

Gene deletion collections, such as those available for fungi (Winzeler et al., 1999), can aid functional analysis of eukaryotic genomes. With this aim, large-scale efforts have generated collections of knockout vectors for *P. falciparum* (Maier et al., 2008) and *Plasmodium berghei* (Gomes et al., 2015), which have led to the functional annotation of dozens of genes in both species. However, similar approaches have not been adapted to *T. gondii*, despite the advantage of both high transfection rates and a continuous culture system. The recent adaptation of clustered regularly interspaced short palindromic repeats (CRISPR)/Cas9 has further enhanced the genetic tractability of *T. gondii* (Shen et al., 2014; Sidik et al., 2014). This technology has the advantage of being easily reprogrammable by changing the 20 bp of homology between the single guide RNA (sgRNA, or guide) and the genomic target (reviewed in Sander and Joung, 2014). The endogenously high rates of non-homologous end-joining (NHEJ) in *T. gondii* make it well suited to CRISPR-mediated gene disruption by efficiently creating frame-shift mutations and insertions at the cleavage site (Sidik et al., 2014).

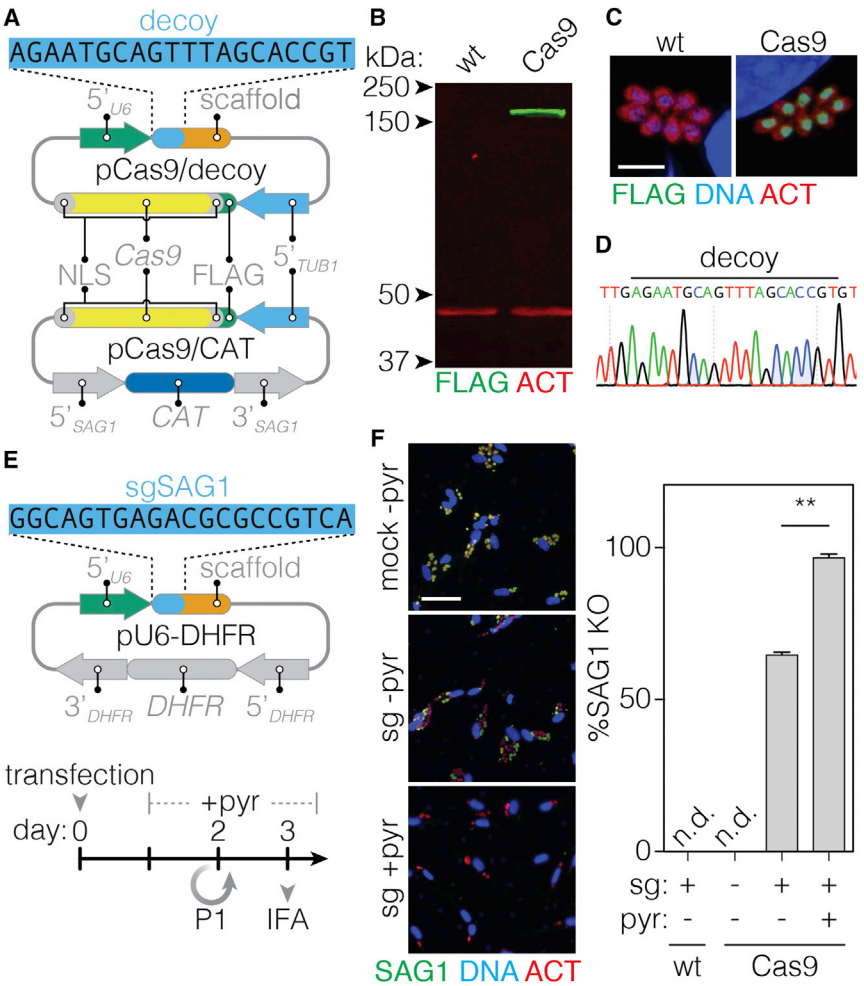

Figure 1. Expression of Cas9 Maximizes Gene Disruption in *T. gondii*

(A) Constructs used to constitutively express Cas9 in *T. gondii*. The sequence of the decoy sgRNA is highlighted (blue), followed by the Cas9-binding scaffold (orange).

(B) Immunoblot showing expression of FLAG-tagged Cas9 (green) in the strain constitutively expressing the transgene. ACT1 serves as a loading control (red).

(C) Cas9 localizes to the parasite nucleus. ACT1 provides a counterstain and DAPI stains for host-cell and parasite nuclei. Scale bar, 10 μm.

(D) Chromatogram showing the presence of the decoy in the Cas9-expressing strain.

(E) The sgRNA expression construct with the pyrimethamine-resistance selectable marker (*DHFR*). The targeting sequence of the *SAG1* sgRNA is highlighted. The timeline indicates the period of pyrimethamine (pyr) selection (if applied), passaging to new host cells (P1), and the immunofluorescence assay (IFA).

(F) Representative micrographs showing intracellular parasites 3 days post-transfection. Parasites were stained for SAG1 (green) and ACT1 (red). Host-cell and parasite nuclei were stained with DAPI (blue). Scale bar, 60 μm. The efficiency of *SAG1* disruption in wild-type and Cas9-expressing parasites was measured following different treatments. Mean ± SD for n = 2 independent experiments; **p < 0.005.

wt, wild-type. n.d., not detected.

Several studies have developed CRISPR/Cas9-based genome-wide genetic screens for mammalian cells (Koike-Yusa et al., 2014; Shalem et al., 2014; Wang et al., 2014). These screens use lentiviral libraries of sgRNAs to generate pools of mutants that can be exposed to selective pressures. The integrated sgRNAs can be used as barcodes to measure the contribution of targeted genes to cell fitness. Despite the lack of viral transduction, we adapted CRISPR/Cas9 for pooled screening in *T. gondii.* We present the first genome-wide genetic screen performed in any apicomplexan. We demonstrate the power of this approach using both positive and negative selection strategies. This approach provides the first complete survey of contributions to parasite fitness, cataloguing the ~40% of genes needed during infection of human fibroblasts. Based on this analysis, we were able to pinpoint previously uncharacterized conserved apicomplexan proteins necessary for the *T. gondii* lytic cycle. We demonstrate that one of these proteins acts as an essential invasion factor and is also required by the malaria parasite *P. falciparum* to complete its asexual replication cycle. This protein is conserved throughout the phylum, providing an important molecular link to the invasion process of distantly related apicomplexans. Our analysis demonstrates the potential of genetic screens in *T. gondii* to uncover conserved biological processes and provides a transformative tool for parasitology.

RESULTS

Constitutive Cas9 Expression Maximizes Gene Disruption in *T. gondii*

Highly efficient gene disruption and stable integration of the sgRNA are necessary to develop large-scale CRISPR screens. Transient expression of *Sp*Cas9 and an sgRNA in *T. gondii* can disrupt a targeted gene in ~20% of parasites (Sidik et al., 2014). We reasoned that constitutive Cas9 expression, prior to introducing the sgRNA, might increase the likelihood of gene disruption. We transfected parasites with a Cas9-expression plasmid carrying a chloramphenicol acetyltransferase (CAT) selectable marker (pCas9/CAT; Figure 1A). However, repeated attempts failed to isolate Cas9-expressing parasites, suggesting that Cas9 expression is detrimental to *T. gondii*, as has been suggested for other microorganisms (Jiang et al., 2014; Peng et al., 2014). We hypothesized that expression of a "decoy" sgRNA (pCas9/decoy; Figure 1A) could prevent toxicity that might arise from unintended Cas9 activity directed by

endogenous RNAs. For this purpose, we used an sgRNA that appeared non-functional against the 3′ UTR of *NHE1*. Co-transfection of pCas9/CAT and pCas9/decoy readily yielded Cas9-expressing parasites, confirmed by immunoblotting (Figure 1B) and immunofluorescence (Figure 1C). As predicted, the Cas9-expressing strain retained the decoy locus (Figure 1D), reinforcing its requirement for constitutive Cas9 expression.

We assessed the efficiency of gene disruption in the Cas9-expressing strain by expressing an sgRNA against the surface antigen *SAG1*. Pyrimethamine treatment of the population selected for stable integration of the sgRNA expression vector (pU6-DHFR), which carries the resistant allele of dihydrofolate reductase (*DHFR*; Figure 1E). SAG1 provides a reliable measure of gene disruption, because it is dispensable yet stably maintained in cultured parasites (Kim and Boothroyd, 1995). 3 days after transfection with the sgRNA construct, 70% of Cas9-expressing parasites had lost SAG1 expression. Pyrimethamine selection further improved SAG1 disruption to 97% over the same time period (Figure 1F). The high efficiency of CRISPR-mediated gene disruption in Cas9-expressing parasites provided the platform for large-scale genetic screens in *T. gondii*.

A Genome-scale Genetic Screen Identifies Genes Involved in Drug Sensitivity

We designed a library of sgRNAs containing ten guides against each of the 8,158 predicted *T. gondii* protein-coding genes using previously described criteria (Wang et al., 2014). The library was cloned into the sgRNA expression vector (Figure 1E). 40% of the parasites that survived transfection integrated the vector into their genomes (data not shown). We could therefore measure the relative abundance of each integrated sgRNA by next-generation sequencing. Since the frequency of a given sgRNA corresponds to the relative abundance of parasites carrying the targeted disruption, the change in relative abundance from the composition of the plasmid library before transfection indicates the enrichment or depletion of a given mutant. We defined the average $\log_2$ fold change in abundance for sgRNAs targeting a given gene as the "phenotype" score for that gene (Figure 2A). To determine whether we could maintain diversity over time, we transfected the library into both wild-type and Cas9-expressing parasites and sampled the populations after each of three lytic cycles (Figure 2B, left). The representation of guides against all genes remained stable over the course of the experiment in the absence of Cas9. In contrast, sgRNAs against specific genes were lost from the Cas9-expressing population (Figure 2C), indicating that a diverse set of mutants had been generated.

To investigate the compatibility of our screen with positive-selection strategies, we treated pools of mutants with 5-fluorodeoxyuridine (FUDR), which is toxic to parasites through its incorporation into pyrimidine pools. Three lytic cycles after transfection with the library, we split the Cas9-expressing parasites into cultures with or without FUDR (Figure 2B, right). As expected, FUDR-treated cultures recovered slowly, and untreated cultures were passaged two or three times over the same period. Measuring the sgRNAs in the two populations revealed that FUDR strongly selected against uracil phosphoribosyltransferase (UPRT) activity, observed as an increased abundance of sgRNAs against *UPRT* and the highly reproducible phenotype score for the gene (Figures 2D and 2E). Since loss of UPRT—a component of the pyrimidine salvage pathway—is known to confer FUDR resistance (Donald and Roos, 1995), this experiment demonstrates the power of this approach to rapidly and efficiently identify positively selected mutants from a *T. gondii* population.

A Genome-scale Genetic Screen Identifies Fitness-Conferring Genes in *T. gondii*

Loss of sgRNAs from a population of mutants can serve to identify genes that contribute to cellular fitness (Wang et al., 2015). In the context of our *T. gondii* screen, the changes in sgRNA representation observed after the third lytic cycle provided a convenient measure of a gene's contribution to fitness. This time point resembled the gene rankings of later cycles (Figure 2F) while minimizing the chance of stochastic guide loss. We calculated the mean phenotype score for each parasite gene from four biological replicates of the screen. Genes that contribute to parasite fitness, represented by negative scores, were distributed throughout the genome and did not segregate by gene length or position on the chromosome (Figure 3A). Gene set enrichment analysis (GSEA) (Croken et al., 2014; Subramanian et al., 2005) showed that genes predicted to be essential, like those encoding ribosomal and proteasomal constituents, were enriched in low phenotype scores (Figure 3B). Genes that encode components of the apicoplast—a plastid common to most apicomplexans—showed a similar enrichment, in accordance with the essential metabolic functions performed by this organelle (Seeber and Soldati-Favre, 2010). In contrast, specialized secretory organelles like the micronemes, dense granules, and rhoptries had fewer genes with low phenotype scores, possibly reflecting functional redundancy or dispensability in cell culture (Figure 3C).

We analyzed the screen results for 81 genes previously reported to be either dispensable or essential for *T. gondii* growth in human fibroblasts (Table S1). The two groups of genes were clearly segregated on the basis of their phenotype scores ($p = 6.7 \times 10^{-16}$), with lower scores for the essential genes (Figure 3D). The most prominent outlier was *RAB4*, which appeared to be essential based on overexpression of a dominant-negative allele (Kremer et al., 2013). However, we readily obtained *RAB4* knockouts that grew normally (Figure S1), demonstrating its dispensability in cell culture. We therefore excluded *RAB4* and, for consistency, other genes classified by overexpression experiments from subsequent analyses. To predict which genes might contribute to parasite fitness, we compared the phenotype score and distribution of sgRNAs for each gene to the values of 40 known dispensable genes. Using 10-fold cross validation on the set of control genes, we estimate this method can classify genes with >95% accuracy. Based on these results, we expect ~40% of *T. gondii* genes significantly contribute to parasite fitness under the conditions tested.

To further classify the fitness-conferring genes, we compared our predictions to other measures of gene function. Genes that are not expressed during the examined developmental stage are more likely to appear dispensable. Accordingly, only 6.9%

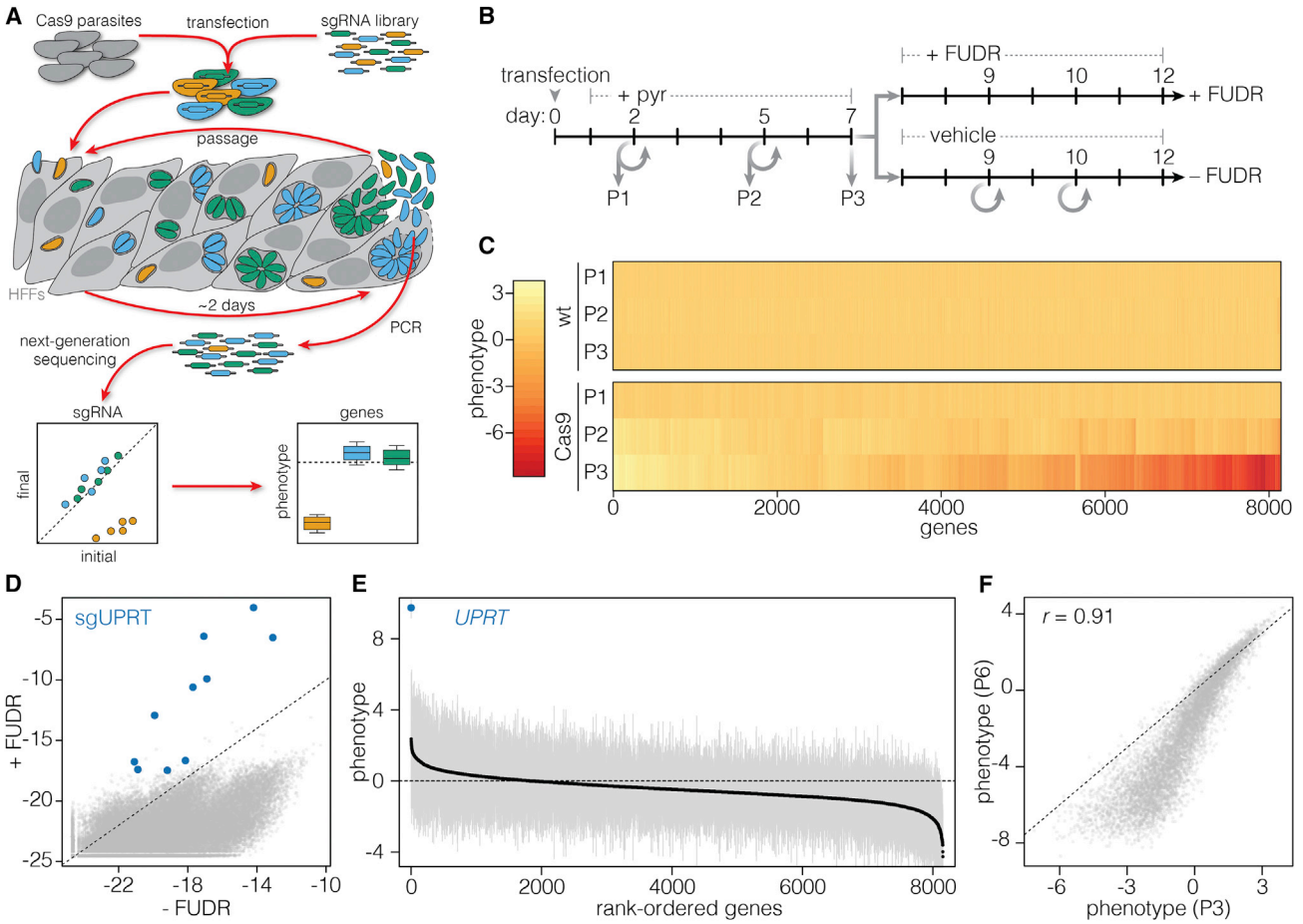

Figure 2. Using Pooled Screens to Identify Genes Responsible for Drug Sensitivity

(A) Schematic depiction of the pooled CRISPR screen. Cas9-expressing parasites are transfected with the sgRNA library and grown in human foreskin fibroblasts (HFFs). At various time points, sgRNAs are amplified and enumerated by sequencing to determine relative abundance and phenotype scores for individual genes.

(B) Timeline for the generation of mutant populations and subsequent selection in the presence or absence of FUDR. Times at which parasites were passaged (P) are indicated.

(C) Heatmap showing the phenotype score of genes at different time-points following transfection of the library into wild-type (wt) or Cas9-expressing parasites.

(D) Relative abundance of sgRNAs following growth of the population in the presence or absence of FUDR. Mean $\log_2$(normalized abundance) for each sgRNA in three independent experiments; sgRNAs against *UPRT* (blue).

(E) Phenotype score calculated for each gene comparing growth ± FUDR. Mean ± SEM for n = 3 independent experiments; *UPRT* (blue).

(F) Comparison of phenotypic scores in untreated samples after three (P3) or six (P6) passages. Pearson's correlation coefficient (*r*) is shown.

of the fitness-conferring genes were found in the lowest quartile of expression, in contrast to 38.6% of genes predicted to be dispensable (Figure 3E). Genes under purifying selection are also more likely to be essential (Jordan et al., 2002). Low ratios of non-synonymous to synonymous mutation rates (d_N/d_S) are consistent with purifying selection. Comparison of syntenic genes between related species or other *T. gondii* strains revealed the expected enrichment for low phenotype scores among genes with low d_N/d_S values (Figures 3F and S2). As an extension of the same principle, genes found in a greater proportion of eukaryotic genomes are more likely to be essential. To test this prediction, we assessed the depth of conservation of *T. gondii* genes using ortholog groupings of 79 eukaryotic genomes available through OrthoMCL DB (Chen et al., 2006). The distribution of phenotype scores within each category followed the predicted trend, which correlated depth of conservation with contribution to fitness and functional annotation (Figure 3G). The strong agreement of our results with published observations and expected trends allows us to confidently predict which genes will contribute to parasite fitness.

Functional Characterization of Fitness-Conferring Genes Conserved in Apicomplexans

We focused our efforts on the ~200 fitness-conferring genes that lacked functional annotation and were only present in apicomplexans, which we called indispensable conserved apicomplexan proteins (ICAPs). We examined the subcellular localization of 28 ICAPs using CRISPR-mediated endogenous tagging to introduce a C-terminal Ty epitope into each targeted gene (Figure 4A). 3 days post-transfection, ~60% of the populations

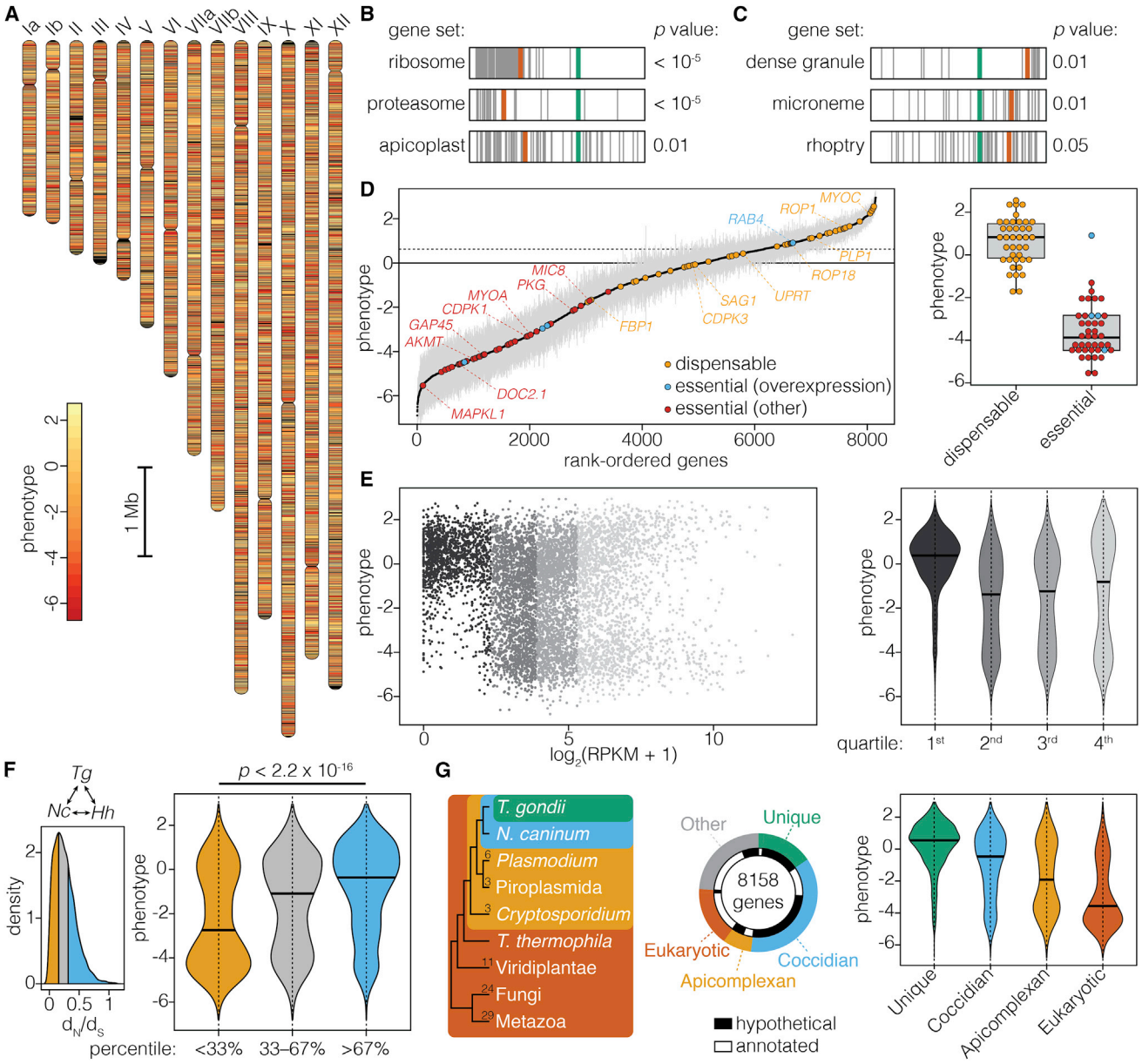

Figure 3. A Genome-scale Screen Measures the Contribution of Each Parasite Gene to Fitness in Human Fibroblasts

(A) Diagram of *T. gondii* chromosomes with genes colored according to phenotype.

(B and C) Significantly enriched (B) or depleted (C) gene sets identified by GSEA. Genes belonging to each category (gray) are plotted according to their rank in the screen, relative to the maximum enrichment score (red) and zero phenotype (green). Phenotype scores for a given set were compared to the entire set by a Kolmogorov-Smirnov test (FDR corrected) to calculate the *p* values.

(D) *T. gondii* genes rank-ordered based on their phenotype. Genes previously reported are highlighted, indicating whether they are dispensable (yellow), or indispensable as inferred from overexpression (blue) or another method (red). Dotted line represents the median phenotype score for the dispensable genes. Mean ± SEM for n = 4 independent experiments. The two groups are compared in a box plot where whiskers indicate the most extreme data within 1.5 times the interquartile range from the boxed quartiles (right).

(E) Correlation of phenotype scores to gene expression based on maximum RPKM values. The distribution of phenotypes in each expression quartile is plotted in the violin graph. Bars indicate the group median.

(F) Analysis of selective pressure for 5,897 syntenic genes found in all three coccidian genomes (*Tg*, *T. gondii*; *Nc*, *N. caninum*; *Hh*, *H. hammondi*). Histogram shows the distribution of d_N/d_S values, highlighting the top and bottom third. Genes binned according to d_N/d_S show higher phenotype scores for genes under purifying selection (orange). Bars indicate the group median. The distributions were compared using a Kolmogorov-Smirnov test.

(G) Correlation between phenotype scores and depth of conservation. The phylogenetic relationship between *T. gondii* and the other genomes used in the analysis is illustrated by the dendrogram, with number of genomes in each taxon indicated. The proportion of *T. gondii* genes and, within this, the proportion that are functionally annotated, are shown for each category. The distribution of phenotype scores for each category is plotted. Bars indicate the group median.

See also Figures S1 and S2 and Tables S1, S2, and S3.

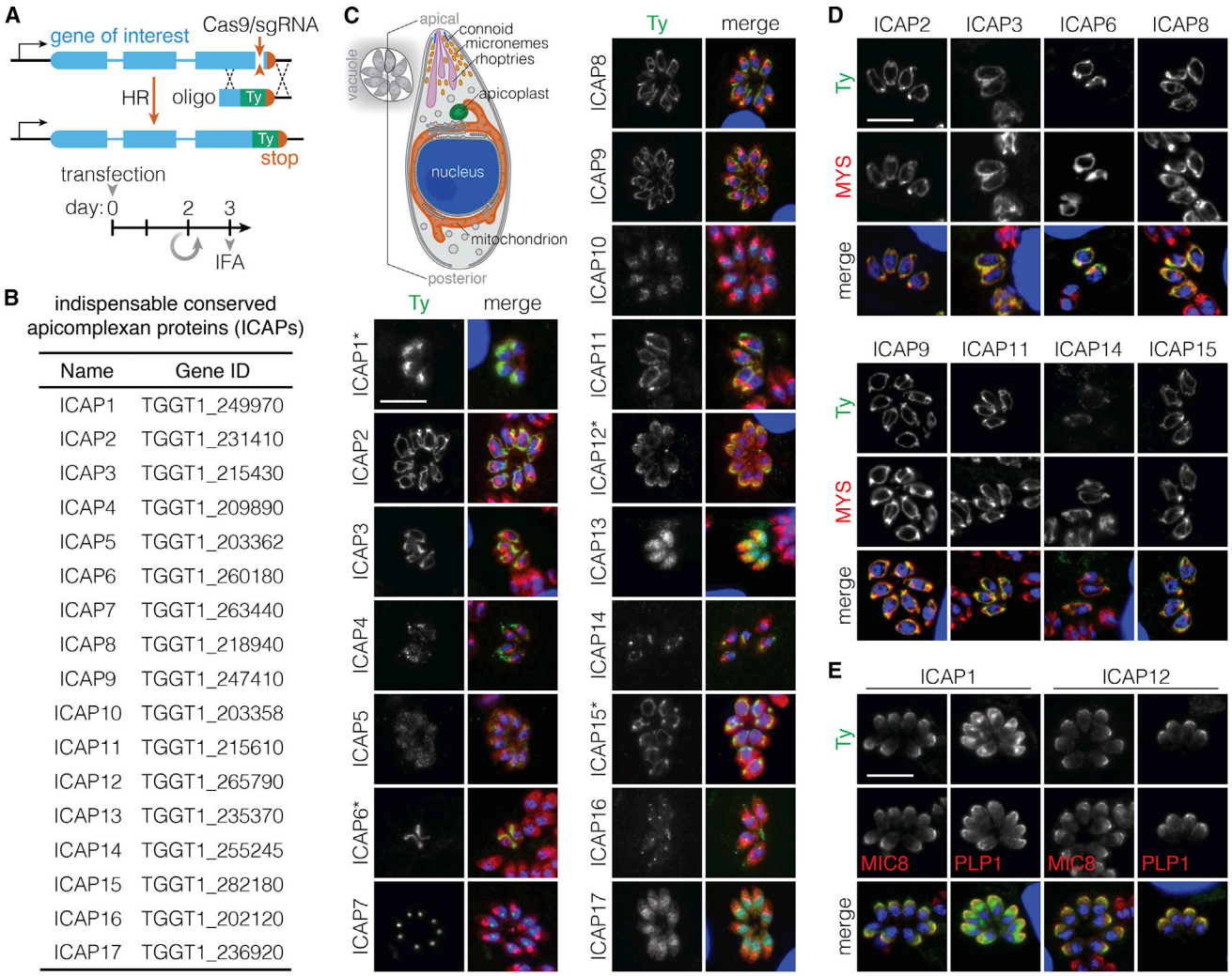

Name	Gene ID
ICAP1	TGGT1_249970
ICAP2	TGGT1_231410
ICAP3	TGGT1_215430
ICAP4	TGGT1_209890
ICAP5	TGGT1_203362
ICAP6	TGGT1_260180
ICAP7	TGGT1_263440
ICAP8	TGGT1_218940
ICAP9	TGGT1_247410
ICAP10	TGGT1_203358
ICAP11	TGGT1_215610
ICAP12	TGGT1_265790
ICAP13	TGGT1_235370
ICAP14	TGGT1_255245
ICAP15	TGGT1_282180
ICAP16	TGGT1_202120
ICAP17	TGGT1_236920

Figure 4. Subcellular Localization of Indispensable Conserved Apicomplexan Proteins

(A) CRISPR was used to introduce a C-terminal Ty tag into the endogenous locus of individual genes through homologous recombination (HR) following the indicated timeline.

(B) List of successfully tagged indispensable conserved apicomplexan proteins (ICAPs), numbered according to their phenotype scores from lowest (ICAP1) to highest (ICAP17).

(C) 3 days after transfection, intracellular parasites were fixed and stained for Ty (green), ACT1 (red), and DAPI (blue). Asterisk denotes fixation in methanol instead of formaldehyde. Scale bar, 10 μm. The diagram illustrates the relative position of various organelles within the parasite.

(D and E) Colocalization ICAPs (green) with a mitochondrial marker (MYS; red) (D) or micronemal proteins (MIC8 or PLP1; red) (E). Nuclei stained with DAPI (blue) are shown in the merged image. Scale bar, 10 μm.

See also Table S2.

displayed Ty expression in 5%–20% of parasite vacuoles (Figures 4B and 4C). Several proteins displayed characteristic structures including secretory vesicles like the micronemes (ICAPs 1 and 12), organelles like the mitochondrion (ICAPs 2, 3, 6, 8, 9, 11, 14, and 15), and compartments like the nucleolus (ICAP7) and conoid (ICAP16) (Figure 4C). Overlap with a known marker of the mitochondrion (MacRae et al., 2012) confirmed the localization of the putative mitochondrial ICAPS (Figure 4D). Both micronemal proteins co-localized with the microneme markers MIC8 (Kessler et al., 2008) and PLP1 (Kafsack et al., 2009) (Figure 4E). ICAP1 was shown to be essential for regulated exocytosis during the preparation of this work (Bullen et al., 2016), confirming our predictions regarding its importance and localization.

To assist the functional characterization of ICAPs, we engineered parasites that stably expressed both Cas9 and a nuclear YFP marker (H2B-YFP) (Hu et al., 2004) for fluorescence microscopy. This strain exhibited a high rate of sgRNA-mediated gene disruption, comparable to the strain used in the screen (Figure S3). As controls, we selected several genes known to be either indispensable (*MYOA* and *CDPK1*) or dispensable (*SAG1*, *PLP1*, and *MYOC*) and five uncharacterized genes predicted to be dispensable by the screen (controls 1–5; Figure 5A).

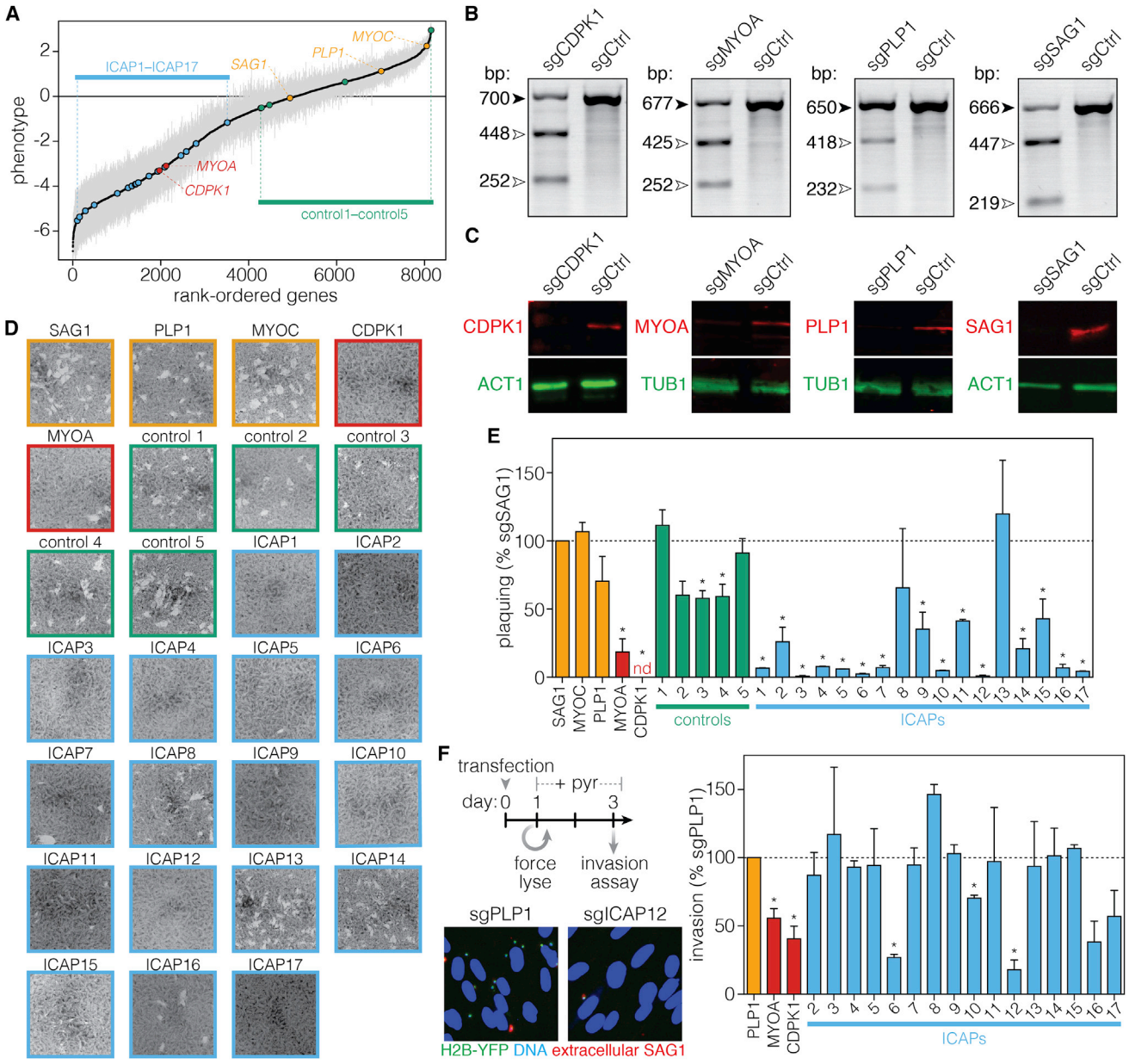

Figure 5. Functional Characterization of Indispensable Conserved Apicomplexan Proteins

(A) Position of analyzed genes within the phenotypic ranking of all *T. gondii* genes. Known indispensable (red) or dispensable (yellow) genes used as controls are indicated. The ICAPs (blue) and uncharacterized genes predicted to be dispensable (green) are numbered in ascending order according to their rank. Mean ± SEM for n = 4 independent experiments.

(B and C) Gene disruption observed at a population level three days after transfection with various control constructs. Disruption of the target locus is observed by Surveyor assay comparing, for each locus, the specific sgRNA to an irrelevant sgRNA against the dispensable gene *MYOC* (B). Loss of the target proteins (red) is observed in samples treated with the targeting sgRNA but not the control, while the loading controls (green) remain unchanged (C).

(D and E) Plaque assays performed immediately following transfection with sgRNAs targeting ICAPs or control genes (D). The number of plaques observed for disruption of each gene relative to the sgRNA against *SAG1* (E). Mean ± SEM for n = 2 independent experiments; *, FDR-adjusted $p < 0.1$ relative to the control.

(F) Secondary screen for genes involved in invasion. The period of intracellular growth prior to phenotypic changes was extended by forced release and passaging the day after transfection. Invasion was assayed after the subsequent lysis, and calculated relative to *PLP1* disruption. Mean ± SEM for n = 2 independent experiments; *, FDR-adjusted $p < 0.1$ relative to the control. Representative immunofluorescence images are shown.

See also Figure S3 and Table S2.

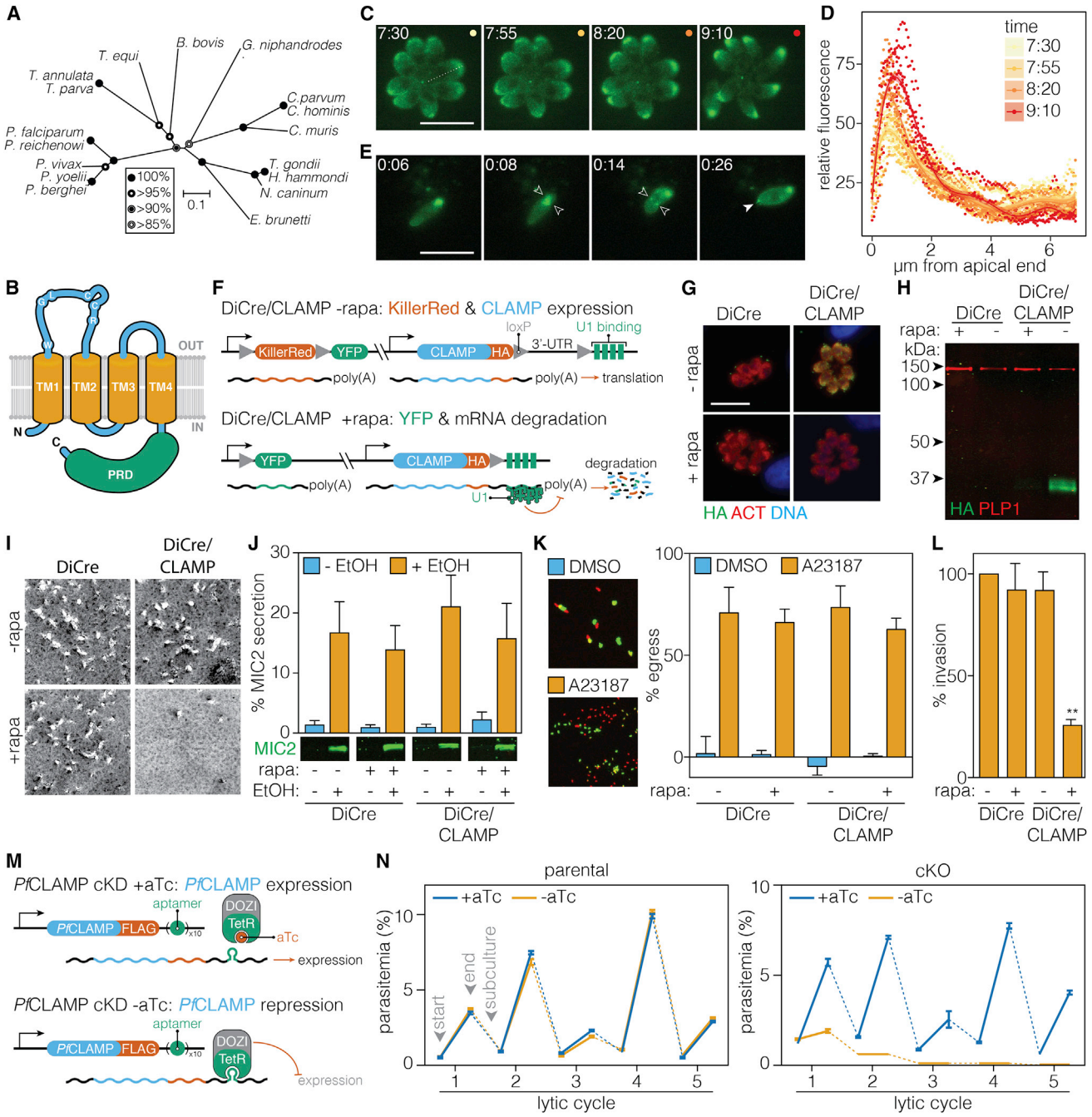

Figure 6. CLAMP Mediates *T. gondii* Invasion and Is Essential for the *P. falciparum* Asexual Cycle

(A) Neighbor-joining tree showing the phylogenetic relationships of *CLAMP* homologs in diverse apicomplexans. Bootstrap values for 10,000 trials are displayed.

(B) Inferred topology of CLAMP highlighting transmembrane domains (orange) and the proline-rich domain (green). See also Figure S4.

(C–E) CLAMP-mNeonGreen localization during egress and invasion. Intracellular parasites expressing CLAMP-mNeonGreen were stimulated to egress with A23187 (C). Relative fluorescence across the length of each parasite (dotted line) is plotted for the four time-points shown. Lines are polynomial regressions ± 95% CI (D). The localization was also monitored during invasion (E). The position of the moving junction is indicated with paired open arrows. Solid arrowhead indicates a punctum of mNeonGreen at the posterior of the parasite appearing immediately after invasion. Time is expressed in minutes:seconds following addition of the compound (C and D) or initiation of invasion (E). Scale bar, 10 µm.

(F) Diagram of the DiCre/CLAMP strain showing how after rapamycin (rapa) treatment the reporter locus switches from expressing KillerRed to expressing YFP, and *CLAMP* mRNA degradation is induced.

(G and H) A 2-hr treatment with rapa is sufficient to induce *CLAMP* degradation as demonstrated by immunofluorescence microscopy 24 hr later (G) or immunoblotting 2 days later (H). The parental strain (DiCre) is included as a control.

(legend continued on next page)

Examining populations of parasites three days after transfection with guides against selected controls showed high rates of on-target mutations (Figure 5B) and significant loss of the target proteins (Figure 5C). Therefore, we can study the effect of a given sgRNA without isolating clonal populations, allowing us to analyze a large set of candidate genes in arrayed, secondary screens.

As an initial measure of gene function, we analyzed plaque formation immediately after transfection with each specific sgRNA construct. Plaques are formed as infection originating from single parasites spreads to adjacent cells clearing a portion of the monolayer, thereby reflecting parasite viability and competency over several lytic cycles. This resulted in reproducible plaque numbers for all sgRNAs against genes known or predicted to be dispensable (Figures 5D and 5E). In contrast, sgRNAs against known essential proteins and most of the ICAPs led to formation of small or significantly fewer plaques (Figures 5D and 5E). These experiments confirm our screen's results and identify several previously uncharacterized genes predicted to be essential for the *T. gondii* lytic cycle.

Invasion of host cells is a central feature of the apicomplexan life cycle. To identify unknown components of the invasion machinery, we investigated the role of ICAPs in this process. The effect of each sgRNA was measured 3 days post-transfection relative to the disruption of *PLP1*, which is known to be dispensable for invasion (Kafsack et al., 2009) (Figure 5F). *MYOA* and *CDPK1* served as positive controls based on their documented phenotypes (Lourido et al., 2010; Meissner et al., 2002). A quarter of the genes tested appeared to impact parasite invasion (Figure 5F). Although this assay could be affected by defects in extracellular survival, slow protein turnover, or sgRNA efficiency, it provides a rapid means to identify candidate invasion factors. ICAP12 had the strongest effect on invasion, which, in light of its micronemal localization, motivated a more detailed characterization.

ICAP12 Is an Invasion Factor Conserved Throughout the Apicomplexa

ICAP12 orthologs were present in all available apicomplexan genomes, and their alignment recapitulated the known relationship between the species (Figure 6A). Topology prediction supports a model with four transmembrane domains and cytoplasmic N and C termini (Figure 6B). The transmembrane domains and extracellular loops are more conserved than the C-terminal proline-rich domains (Figure S4). No related sequences could be identified outside the Apicomplexa. However, hidden Markov model-based searches suggest structural similarity between ICAP12 and the mammalian tight-junction proteins claudin-15 and claudin-19. Based on these features and its localization, we named ICAP12 "claudin-like apicomplexan microneme protein" (CLAMP).

We tagged the endogenous *CLAMP* locus with mNeonGreen to study its localization in vivo. The fusion protein concentrated at the apical end of parasites, consistent with micronemal localization (Figure 6C). Micronemes are secreted in response to increased cytosolic Ca^{2+}, which mediates parasite motility, egress, and invasion of host cells (Carruthers et al., 1999). We monitored CLAMP localization following stimulation with the Ca^{2+} ionophore A23187 and observed increased apical fluorescence prior to egress (Figures 6C and 6D; Movie S1). Following incubation with host cells, formation of CLAMP foci could be detected at the posterior of most parasites (Figure S5A). We also observed active formation of such foci during invasion (Figure 6E, arrowheads; Movie S2). This relocalization of CLAMP is similar to what has been observed for other membrane-tethered micronemal proteins (Carruthers and Sibley, 1999; Garcia-Réguet et al., 2000).

To directly examine CLAMP function, we used a conditional gene-silencing method (Pieperhoff et al., 2015). In a strain expressing a rapamycin-dimerizable version of the Cre recombinase (DiCre), we modified the endogenous *CLAMP* locus to include a C-terminal hemagglutinin (HA) tag and a floxed 3′ UTR followed by four U1-binding sequences (DiCre/CLAMP; Figure 6F). Rapamycin treatment triggers excision of the 3′ UTR and U1-mediated mRNA degradation. The strain also carries a reporter that switches expression of KillerRed for YFP upon Cre activation. A 2-hr rapamycin treatment during initial infection efficiently downregulated CLAMP expression (green), as measured by immunofluorescence 24 hr later (Figure 6G) or by immunoblot 2 days later (Figure 6H). To determine the impact of CLAMP on the lytic cycle, we examined plaque formation following treatment with rapamycin. The treatment did not affect the parental strain (DiCre; Figure 6I). However, CLAMP silencing blocked plaque formation, and the few plaques remaining likely represent the 5%–10% of parasites that do not undergo recombination (DiCre/CLAMP; Figure 6I).

To determine the precise defect associated with CLAMP loss, we examined several stages of the lytic cycle. We tested whether CLAMP downregulation might affect microneme secretion, which can be experimentally triggered by ethanol treatment (Carruthers et al., 1999). Rapid shedding of micronemal adhesins from the parasite surface allows quantification of secretion by measuring protein accumulation in the supernatant. Comparing the relative abundance of secreted MIC2—a micronemal adhesin—demonstrates that CLAMP silencing has no effect on microneme secretion (Figure 6J). We also observed normal motility and egress when intracellular parasites were treated with A23187 (Figure 6K) or the phosphodiesterase inhibitor zaprinast (Movie S3). Following stimulated egress, parasites

(I–L) The DiCre/CLAMP strain or its parental stain (DiCre) was treated as above. Parasites were harvested and phenotypically assayed for plaque formation (I), microneme secretion (J), egress (K), or invasion (L). Secretion was measured as the percentage of total MIC2 present in the parasites (J). Egress was induced with A23187 and compared to a vehicle control (DMSO) over the same period (K). All results are means ± SEM for n = 3 independent experiments; $^{**}p < 0.005$ relative to the untreated DiCre strain.

(M) Diagram of the *Pf*CLAMP cKD showing how removing aTc allows the TetR-DOZI regulator to bind and suppress expression.

(N) Growth curves of the parental strain (left) or the cKD (right) ± aTc. Means ± SD for n = 3 technical replicates. See also Figure S5D for an independent replicate. See also Figures S4 and S5 and Movies S1, S2, S3, and S4.

frequently reinvade adjacent host cells. However, CLAMP silencing rendered reinvasion attempts unsuccessful (Movie S4). These events were characterized by repetitive parasite thrusting motion and deformation. To directly measure this defect, CLAMP was silenced during the growth cycle prior to the assaying invasion. Knockdown of CLAMP had a profound effect on invasion, reducing the number of intracellular parasites by 80% (Figure 6L). These results implicate CLAMP in the cellular events immediately preceding invasion of host cells.

CLAMP Is Essential during the Asexual Cycle of Malaria

To test whether the essentiality of CLAMP extends to other apicomplexans, we constructed a conditional knockdown (cKD) of its ortholog in *P. falciparum*. We tagged the endogenous locus of *Pf*CLAMP with a FLAG epitope tag and ten tandem aptamer sequences, which bind the Tet repressor protein (TetR) when transcribed (Ganesan et al., 2016). TetR is expressed as a fusion with the translational repressor (DOZI) in the same strain, which suppresses expression of the aptamer-tagged transcript unless anhydrotetracycline (aTc) is added to the media (Figure 6M). We confirmed correct integration of the construct into the *Pf*CLAMP locus by sequencing (Figures S5B and S5C). To test the effect of CLAMP repression on the asexual cycle of *P. falciparum*, we passaged the parasites into cultures that either contained or lacked aTc. The different conditions had no effect on the growth of the parental strain (Figure 6N, left). In contrast, withdrawal of aTc from the *Pf*CLAMP cKD led to a rapid and complete block in the asexual cycle (Figure 6N, right). These results demonstrate the essentiality of CLAMP in a second apicomplexan species.

DISCUSSION

We present the first genome-wide functional analysis of an apicomplexan. Using CRISPR/Cas9, we targeted all annotated protein-coding genes in the *T. gondii* genome to generate mutant populations for screens based on positive or negative selection. This method enabled rapid identification of genes that mediate infection of human fibroblasts or confer drug sensitivity. Our results agree with published observations, follow expected genomic trends, and provide new robust predictions that identify several essential proteins conserved throughout the phylum. We also demonstrate that this method can easily identify mutants resistant to the antiparasitic compound FUDR. For such special cases where gene disruption can mediate resistance, our method will facilitate the identification of drug-resistance pathways and provide a complementary approach to mapping spontaneous resistance mutations (Flannery et al., 2013).

Essential apicomplexan adaptations represent ideal targets for therapeutic or prophylactic interventions. However, genes involved in such pathways are difficult to identify. Based on results from our genome-wide screen, we characterized 17 ICAPs. Individually disrupted, most ICAPs could be shown to independently contribute to growth in fibroblasts. None of the ICAPs have defined domains or resemble proteins outside the phylum, yet most of them localized to distinct subcellular structures, assuming no detrimental effect of epitope tagging on localization. Of the eight that localized to the mitochondrion, only ICAP3 and ICAP14 have predicted signal peptides that might have suggested their compartmentalization. Nonetheless, the preponderance of mitochondrial ICAPs and their conservation in several branches of the Apicomplexa suggest that this organelle might serve as a focal point for functions conserved across the phylum, in addition to the currently appreciated genus-specific modifications (Seeber et al., 2008). Two other ICAPs localized to apical secretory vesicles called micronemes, which are more typically associated with specific apicomplexan adaptations. During the preparation of this paper, the first, ICAP1 (APH), was shown to be required for microneme secretion (Bullen et al., 2016). The second one, ICAP12, was critically important for invasion, as demonstrated by our secondary screens and subsequent analysis. These data argue for an in-depth examination of other ICAPs, which will likely reveal essential processes conserved among apicomplexans.

We renamed ICAP12 CLAMP to reflect its subcellular localization and structural similarity to mammalian claudins. Conditional silencing demonstrated that CLAMP is specifically required during invasion of host cells and did not affect microneme secretion or dependent processes. CLAMP is thereby distinct from factors that participate in both gliding motility and invasion (Bargieri et al., 2014). Instead, CLAMP resembles factors involved in the formation of the tight junction—or moving junction—through which parasites enter host cells. Knockdown of the micronemal protein MIC8 resembles CLAMP disruption by blocking secretion of the rhoptry neck proteins that anchor the micronemal adhesin AMA1 to the host cell membrane (Kessler et al., 2008). Video microscopy showed CLAMP-deficient parasites repeatedly pushing against the host-cell membrane while failing to initiate invasion, much like *P. falciparum* parasites unable to form a moving-junction (Treeck et al., 2009). Apposition of the parasite and host-cell membrane is a hallmark of apicomplexan parasitism, mediating discharge of rhoptry contents into host cells and complete or partial invasion (Bargieri et al., 2014). Despite the similarities, previously identified invasion factors are not completely conserved throughout the phylum; MIC8 is restricted to the coccidia, and AMA1 and RON2, which are central components of the moving junction, are absent from early branching apicomplexans (EupathDB). In contrast, CLAMP homologs are found in all sequenced apicomplexan genomes, including early branching members like cryptosporidians and gregarines. Consistent with its conservation, the ortholog of CLAMP in *P. falciparum* could be readily identified, and its knockdown leads to a complete inhibition of the asexual cycle, although further work will be necessary to define its precise function. These results argue for a pivotal role of CLAMP in all members of the phylum. Its structural resemblance to mammalian claudins suggests the physical involvement of CLAMP in tight-junction formation during invasion. Claudins are known to engage in homotypic and heterotypic interactions, as well as the formation of paracellular channels that restrict the flow of ions across the tight junction (Krause et al., 2008). Whether CLAMP participates in similar processes remains speculative, but its study might shed light into one of the most conserved features of apicomplexan parasitism.

By screening for genes that confer parasite fitness during growth in human fibroblasts, we provide a baseline for gene

function under arguably permissive conditions. Future screens will need to define the genes required during other life stages, in different hosts, under varying nutrient conditions, and in response to immune pressures. The potential to obscure or exacerbate deleterious mutations in pooled screens due to competition with wild-type parasites should be mentioned here. However, this screening format has the advantage of simultaneously determining the fate of hundreds of independently generated mutants for a given gene. As such, they are less influenced by rare compensatory mutations that can confound interpretation of outcomes when using clonal strains (Lamarque et al., 2014; Ma et al., 2008). Studies in yeast have revealed that adaptations can overcome the need for ~9% of genes previously considered essential (Liu et al., 2015). These issues argue for a nuanced view of gene essentiality. Although our experiments demonstrate the strong predictive value of this method, careful follow-up experiments are necessary to fully explore the role of individual genes.

Genome-wide functional analyses have transformed the study of many organisms. We demonstrate the power of this approach to identify genes that contribute to *T. gondii* fitness during infection of human fibroblasts. Although important adaptations distinguish different parasite genera, this method provides a unique tool to model conserved apicomplexan processes in *T. gondii*, and its success is demonstrated by the identification of a previously uncharacterized protein essential for the malaria parasite *P. falciparum.* Coupled with the diverse tools available for genetic and chemical manipulation of *T. gondii*, the genome-wide screens will provide a framework for the systematic examination of genetic interactions. The unconstrained study of apicomplexan genomes will help us understand their unique biology and broaden the scope of interventions to control these widespread parasitic infections.

STAR★METHODS

Detailed methods are provided in the online version of this paper and include the following:

- KEY RESOURCES TABLE
- CONTACT FOR REAGENT AND RESOURCE SHARING
- EXPERIMENTAL MODEL AND SUBJECT DETAILS
- METHOD DETAILS
  - Plasmid Design and Construction
  - Library Design and Construction
  - *T. gondii* Strain Generation
  - Pooled CRISPR Screens
  - RT-PCR
  - Functional Analysis of ICAPs and Controls
  - ICAP Tagging
  - CLAMP Phylogeny and Topology Predictions
  - CLAMP Conditional Knockdown
  - Immunofluorescence Microscopy and Immunoblotting
  - Surveyor Assays
  - Plaque Formation
  - Microneme Secretion
  - Egress Assays
  - Invasion Assays
  - Video Microscopy
  - *P. falciparum* Strain Generation and Analysis
- QUANTIFICATION AND STATISTICAL ANALYSIS
  - Bioinformatic Analysis of the Screening Results
  - Statistical Testing
- DATA AND SOFTWARE AVAILABILITY
  - Software
  - Data Resources

SUPPLEMENTAL INFORMATION

Supplemental Information includes five figures, three tables, and four movies and can be found with this article online at http://dx.doi.org/10.1016/j.cell.2016.08.019

AUTHOR CONTRIBUTIONS

S.M.S., D.H., and S.L. conceived this study and performed most of the experiments. S.M.G., A.S.N., and J.C.N. designed and performed the malaria work. M.-H.H. and V.B.C. provided essential reagents and insight. T.W. provided the scripts to design the library, which P.T. adapted and executed. J.P.J.S. advised the experimental design and drafting of the manuscript. S.M.S., D.H., and S.L. wrote the manuscript, which was read and approved by all authors.

ACKNOWLEDGMENTS

We thank Emily Shortt for technical support; George Bell for bioinformatics advice; L. David Sibley, Dominique Soldati-Favre, and Lilach Sheiner for the SAG1, MIC8, MYOA, and MYS antibodies; Ke Hu for the NeonGreen plasmid; David S. Roos and Maria Alejandra Diaz-Miranda for the RNA-sequencing data; Markus Meissner for the DiCre strain; and Gail Eskes for naming CLAMP. This work would not have been possible without EupathDB, and we thank all members of the community who have worked to generate this resource. This work was supported by NIGMS Center for Integrative Synthetic Biology Grant P50GM098792, NIH National Research Service Award F31 CA189437 to T.W., NIH Research Project Grant R01AI46675 to V.B.C., and the NIH Director's New Innovator Award 1DP2OD007124 to J.C.N. and Early Independence Award 1DP5OD017892 to S.L.

Received: May 19, 2016
Revised: July 25, 2016
Accepted: August 5, 2016
Published: September 1, 2016

REFERENCES

Achbarou, A., Mercereau-Puijalon, O., Autheman, J.M., Fortier, B., Camus, D., and Dubremetz, J.F. (1991). Characterization of microneme proteins of Toxoplasma gondii. Mol. Biochem. Parasitol. *47*, 223–233.

Bargieri, D., Lagal, V., Andenmatten, N., Tardieux, I., Meissner, M., and Ménard, R. (2014). Host cell invasion by apicomplexan parasites: the junction conundrum. PLoS Pathog. *10*, e1004273.

Bastin, P., Bagherzadeh, Z., Matthews, K.R., and Gull, K. (1996). A novel epitope tag system to study protein targeting and organelle biogenesis in Trypanosoma brucei. Mol. Biochem. Parasitol. *77*, 235–239.

Bullen, H.E., Jia, Y., Yamaryo-Botté, Y., Bisio, H., Zhang, O., Jemelin, N.K., Marq, J.-B., Carruthers, V., Botté, C.Y., and Soldati-Favre, D. (2016). Phosphatidic Acid-Mediated Signaling Regulates Microneme Secretion in Toxoplasma. Cell Host Microbe *19*, 349–360.

Burg, J.L., Perelman, D., Kasper, L.H., Ware, P.L., and Boothroyd, J.C. (1988). Molecular analysis of the gene encoding the major surface antigen of Toxoplasma gondii. J. Immunol. *141*, 3584–3591.

Carruthers, V.B., and Sibley, L.D. (1999). Mobilization of intracellular calcium stimulates microneme discharge in Toxoplasma gondii. Mol. Microbiol. *31*, 421–428.

Carruthers, V.B., Moreno, S.N., and Sibley, L.D. (1999). Ethanol and acetaldehyde elevate intracellular [Ca2+] and stimulate microneme discharge in Toxoplasma gondii. Biochem. J. *342*, 379–386.

Checkley, W., White, A.C., Jr., Jaganath, D., Arrowood, M.J., Chalmers, R.M., Chen, X.-M., Fayer, R., Griffiths, J.K., Guerrant, R.L., Hedstrom, L., et al. (2015). A review of the global burden, novel diagnostics, therapeutics, and vaccine targets for cryptosporidium. Lancet Infect. Dis. *15*, 85–94.

Chen, F., Mackey, A.J., Stoeckert, C.J., Jr., and Roos, D.S. (2006). OrthoMCL-DB: querying a comprehensive multi-species collection of ortholog groups. Nucleic Acids Res. *34*, D363–D368.

Crabb, B.S., de Koning-Ward, T.F., and Gilson, P.R. (2011). Toward forward genetic screens in malaria-causing parasites using the piggyBac transposon. BMC Biol. *9*, 21.

Croken, M.M., Qiu, W., White, M.W., and Kim, K. (2014). Gene Set Enrichment Analysis (GSEA) of Toxoplasma gondii expression datasets links cell cycle progression and the bradyzoite developmental program. BMC Genomics *15*, 515.

Dobrowolski, J.M., Carruthers, V.B., and Sibley, L.D. (1997). Participation of myosin in gliding motility and host cell invasion by Toxoplasma gondii. Mol. Microbiol. *26*, 163–173.

Dobson, L., Reményi, I., and Tusnády, G.E. (2015). CCTOP: a Consensus Constrained TOPology prediction web server. Nucleic Acids Res. *43* (W1), W408–W412.

Donald, R.G., and Roos, D.S. (1993). Stable molecular transformation of Toxoplasma gondii: a selectable dihydrofolate reductase-thymidylate synthase marker based on drug-resistance mutations in malaria. Proc. Natl. Acad. Sci. USA *90*, 11703–11707.

Donald, R.G., and Roos, D.S. (1995). Insertional mutagenesis and marker rescue in a protozoan parasite: cloning of the uracil phosphoribosyltransferase locus from Toxoplasma gondii. Proc. Natl. Acad. Sci. USA *92*, 5749–5753.

Farrell, A., Coleman, B.I., Benenati, B., Brown, K.M., Blader, I.J., Marth, G.T., and Gubbels, M.-J. (2014). Whole genome profiling of spontaneous and chemically induced mutations in Toxoplasma gondii. BMC Genomics *15*, 354.

Flannery, E.L., Fidock, D.A., and Winzeler, E.A. (2013). Using genetic methods to define the targets of compounds with antimalarial activity. J. Med. Chem. *56*, 7761–7771.

Frénal, K., Marq, J.-B., Jacot, D., Polonais, V., and Soldati-Favre, D. (2014). Plasticity between MyoC- and MyoA-glideosomes: an example of functional compensation in Toxoplasma gondii invasion. PLoS Pathog. *10*, e1004504.

Ganesan, S.M., Falla, A., Goldfless, S.J., Nasamu, A.S., and Niles, J.C. (2016). Synthetic RNA-protein modules integrated with native translation mechanisms to control gene expression in malaria parasites. Nat. Commun. *7*, 10727.

Garcia-Réguet, N., Lebrun, M., Fourmaux, M.N., Mercereau-Puijalon, O., Mann, T., Beckers, C.J., Samyn, B., Van Beeumen, J., Bout, D., and Dubremetz, J.F. (2000). The microneme protein MIC3 of Toxoplasma gondii is a secretory adhesin that binds to both the surface of the host cells and the surface of the parasite. Cell. Microbiol. *2*, 353–364.

Goldman, N., and Yang, Z. (1994). A codon-based model of nucleotide substitution for protein-coding DNA sequences. Mol. Biol. Evol. *11*, 725–736.

Gomes, A.R., Bushell, E., Schwach, F., Girling, G., Anar, B., Quail, M.A., Herd, C., Pfander, C., Modrzynska, K., Rayner, J.C., and Billker, O. (2015). A genome-scale vector resource enables high-throughput reverse genetic screening in a malaria parasite. Cell Host Microbe *17*, 404–413.

Hu, K., Roos, D.S., Angel, S.O., and Murray, J.M. (2004). Variability and heritability of cell division pathways in Toxoplasma gondii. J. Cell Sci. *117*, 5697–5705.

Huynh, M.-H., and Carruthers, V.B. (2009). Tagging of endogenous genes in a Toxoplasma gondii strain lacking Ku80. Eukaryot. Cell *8*, 530–539.

Ingram, J.R., Knockenhauer, K.E., Markus, B.M., Mandelbaum, J., Ramek, A., Shan, Y., Shaw, D.E., Schwartz, T.U., Ploegh, H.L., and Lourido, S. (2015). Allosteric activation of apicomplexan calcium-dependent protein kinases. Proc. Natl. Acad. Sci. USA *112*, E4975–E4984.

Jiang, W., Brueggeman, A.J., Horken, K.M., Plucinak, T.M., and Weeks, D.P. (2014). Successful transient expression of Cas9 and single guide RNA genes in Chlamydomonas reinhardtii. Eukaryot. Cell *13*, 1465–1469.

Jordan, I.K., Rogozin, I.B., Wolf, Y.I., and Koonin, E.V. (2002). Essential genes are more evolutionarily conserved than are nonessential genes in bacteria. Genome Res. *12*, 962–968.

Kafsack, B.F.C., Pena, J.D.O., Coppens, I., Ravindran, S., Boothroyd, J.C., and Carruthers, V.B. (2009). Rapid membrane disruption by a perforin-like protein facilitates parasite exit from host cells. Science *323*, 530–533.

Kelley, L.A., Mezulis, S., Yates, C.M., Wass, M.N., and Sternberg, M.J.E. (2015). The Phyre2 web portal for protein modeling, prediction and analysis. Nat. Protoc. *10*, 845–858.

Kessler, H., Herm-Götz, A., Hegge, S., Rauch, M., Soldati-Favre, D., Frischknecht, F., and Meissner, M. (2008). Microneme protein 8–a new essential invasion factor in Toxoplasma gondii. J. Cell Sci. *121*, 947–956.

Kim, K., and Boothroyd, J.C. (1995). Toxoplasma gondii: stable complementation of sag1 (p30) mutants using SAG1 transfection and fluorescence-activated cell sorting. Exp. Parasitol. *80*, 46–53.

Koike-Yusa, H., Li, Y., Tan, E.-P., Velasco-Herrera, Mdel.C., and Yusa, K. (2014). Genome-wide recessive genetic screening in mammalian cells with a lentiviral CRISPR-guide RNA library. Nat. Biotechnol. *32*, 267–273.

Krause, G., Winkler, L., Mueller, S.L., Haseloff, R.F., Piontek, J., and Blasig, I.E. (2008). Structure and function of claudins. Biochimica Et Biophysica Acta (BBA) -. Biomembranes *1778*, 631–645.

Kremer, K., Kamin, D., Rittweger, E., Wilkes, J., Flammer, H., Mahler, S., Heng, J., Tonkin, C.J., Langsley, G., Hell, S.W., et al. (2013). An overexpression screen of Toxoplasma gondii Rab-GTPases reveals distinct transport routes to the micronemes. PLoS Pathog. *9*, e1003213–e1003216.

Lamarque, M.H., Roques, M., Kong-Hap, M., Tonkin, M.L., Rugarabamu, G., Marq, J.-B., Penarete-Vargas, D.M., Boulanger, M.J., Soldati-Favre, D., and Lebrun, M. (2014). Plasticity and redundancy among AMA-RON pairs ensure host cell entry of Toxoplasma parasites. Nat. Commun. *5*, 4098.

Larkin, M.A., Blackshields, G., Brown, N.P., Chenna, R., McGettigan, P.A., McWilliam, H., Valentin, F., Wallace, I.M., Wilm, A., Lopez, R., et al. (2007). Clustal W and Clustal X version 2.0. Bioinformatics *23*, 2947–2948.

Levine, N.D. (1988). The Protozoan Phylum Apicomplexa, *Volume I* (CRC Press, Inc.).

Liu, G., Yong, M.Y.J., Yurieva, M., Srinivasan, K.G., Liu, J., Lim, J.S.Y., Poidinger, M., Wright, G.D., Zolezzi, F., Choi, H., et al. (2015). Gene essentiality is a quantitative property linked to cellular evolvability. Cell *163*, 1388–1399.

Lorenzi, H., Khan, A., Behnke, M.S., Namasivayam, S., Swapna, L.S., Hadjithomas, M., Karamycheva, S., Pinney, D., Brunk, B.P., Ajioka, J.W., et al. (2016). Local admixture of amplified and diversified secreted pathogenesis determinants shapes mosaic Toxoplasma gondii genomes. Nat. Commun. *7*, 10147.

Lourido, S., Shuman, J., Zhang, C., Shokat, K.M., Hui, R., and Sibley, L.D. (2010). Calcium-dependent protein kinase 1 is an essential regulator of exocytosis in Toxoplasma. Nature *465*, 359–362.

Lourido, S., Tang, K., and Sibley, L.D. (2012). Distinct signalling pathways control Toxoplasma egress and host-cell invasion. EMBO J. *31*, 4524–4534.

Ma, C., Tran, J., Li, C., Ganesan, L., Wood, D., and Morrissette, N. (2008). Secondary mutations correct fitness defects in Toxoplasma gondii with dinitroaniline resistance mutations. Genetics *180*, 845–856.

MacRae, J.I., Sheiner, L., Nahid, A., Tonkin, C., Striepen, B., and McConville, M.J. (2012). Mitochondrial metabolism of glucose and glutamine is required for intracellular growth of Toxoplasma gondii. Cell Host Microbe *12*, 682–692.

Maier, A.G., Rug, M., O'Neill, M.T., Brown, M., Chakravorty, S., Szestak, T., Chesson, J., Wu, Y., Hughes, K., Coppel, R.L., et al. (2008). Exported proteins required for virulence and rigidity of Plasmodium falciparum-infected human erythrocytes. Cell *134*, 48–61.

Meier, A., and Söding, J. (2015). Automatic prediction of protein 3D structures by probabilistic multi-template homology modeling. PLoS Comput. Biol. *11*, e1004343.

Meissner, M., Schlüter, D., and Soldati, D. (2002). Role of Toxoplasma gondii myosin A in powering parasite gliding and host cell invasion. Science *298*, 837–840.

Pappas, G., Roussos, N., and Falagas, M.E. (2009). Toxoplasmosis snapshots: global status of Toxoplasma gondii seroprevalence and implications for pregnancy and congenital toxoplasmosis. Int. J. Parasitol. *39*, 1385–1394.

Peng, D., Kurup, S.P., Yao, P.Y., Minning, T.A., and Tarleton, R.L. (2014). CRISPR-Cas9-mediated single-gene and gene family disruption in Trypanosoma cruzi. MBio *6*, e02097-14.

Pieperhoff, M.S., Pall, G.S., Jiménez-Ruiz, E., Das, S., Melatti, C., Gow, M., Wong, E.H., Heng, J., Müller, S., Blackman, M.J., and Meissner, M. (2015). Conditional U1 gene silencing in Toxoplasma gondii. PLoS ONE *10*, e0130356.

Saeij, J.P.J., Boyle, J.P., Coller, S., Taylor, S., Sibley, L.D., Brooke-Powell, E.T., Ajioka, J.W., and Boothroyd, J.C. (2006). Polymorphic secreted kinases are key virulence factors in toxoplasmosis. Science *314*, 1780–1783.

Sander, J.D., and Joung, J.K. (2014). CRISPR-Cas systems for editing, regulating and targeting genomes. Nat. Biotechnol. *32*, 347–355.

Schindelin, J., Arganda-Carreras, I., Frise, E., Kaynig, V., Longair, M., Pietzsch, T., Preibisch, S., Rueden, C., Saalfeld, S., Schmid, B., et al. (2012). Fiji: an open-source platform for biological-image analysis. Nat. Methods *9*, 676–682.

Seeber, F., and Soldati-Favre, D. (2010). Metabolic Pathways in the Apicoplast of Apicomplexa (Elsevier), pp. 161–228.

Seeber, F., Limenitakis, J., and Soldati-Favre, D. (2008). Apicomplexan mitochondrial metabolism: a story of gains, losses and retentions. Trends Parasitol. *24*, 468–478.

Shalem, O., Sanjana, N.E., Hartenian, E., Shi, X., Scott, D.A., Mikkelsen, T.S., Heckl, D., Ebert, B.L., Root, D.E., Doench, J.G., and Zhang, F. (2014). Genome-scale CRISPR-Cas9 knockout screening in human cells. Science *343*, 84–87.

Sheiner, L., Demerly, J.L., Poulsen, N., Beatty, W.L., Lucas, O., Behnke, M.S., White, M.W., and Striepen, B. (2011). A systematic screen to discover and analyze apicoplast proteins identifies a conserved and essential protein import factor. PLoS Pathog. *7*, e1002392.

Shen, B., Brown, K.M., Lee, T.D., and Sibley, L.D. (2014). Efficient gene disruption in diverse strains of Toxoplasma gondii using CRISPR/CAS9. MBio *5*, e01114-14.

Sidik, S.M., Hackett, C.G., Tran, F., Westwood, N.J., and Lourido, S. (2014). Efficient genome engineering of Toxoplasma gondii using CRISPR/Cas9. PLoS ONE *9*, e100450.

Simske, J.S. (2013). Claudins reign: the claudin/EMP/PMP22/γ channel protein family in C. elegans. Tissue Barriers *1*, e25502.

Soldati, D., and Boothroyd, J.C. (1993). Transient transfection and expression in the obligate intracellular parasite Toxoplasma gondii. Science *260*, 349–352.

Subramanian, A., Tamayo, P., Mootha, V.K., Mukherjee, S., Ebert, B.L., Gillette, M.A., Paulovich, A., Pomeroy, S.L., Golub, T.R., Lander, E.S., and Mesirov, J.P. (2005). Gene set enrichment analysis: a knowledge-based approach for interpreting genome-wide expression profiles. Proc. Natl. Acad. Sci. USA *102*, 15545–15550.

Taylor, S., Barragan, A., Su, C., Fux, B., Fentress, S.J., Tang, K., Beatty, W.L., Hajj, H.E., Jerome, M., Behnke, M.S., et al. (2006). A secreted serine-threonine kinase determines virulence in the eukaryotic pathogen Toxoplasma gondii. Science *314*, 1776–1780.

Treeck, M., Zacherl, S., Herrmann, S., Cabrera, A., Kono, M., Struck, N.S., Engelberg, K., Haase, S., Frischknecht, F., Miura, K., et al. (2009). Functional analysis of the leading malaria vaccine candidate AMA-1 reveals an essential role for the cytoplasmic domain in the invasion process. PLoS Pathog. *5*, e1000322.

Wang, T., Wei, J.J., Sabatini, D.M., and Lander, E.S. (2014). Genetic screens in human cells using the CRISPR-Cas9 system. Science *343*, 80–84.

Wang, T., Birsoy, K., Hughes, N.W., Krupczak, K.M., Post, Y., Wei, J.J., Lander, E.S., and Sabatini, D.M. (2015). Identification and characterization of essential genes in the human genome. Science *350*, 1096–1101.

Wellems, T.E., Walker-Jonah, A., and Panton, L.J. (1991). Genetic mapping of the chloroquine-resistance locus on Plasmodium falciparum chromosome 7. Proc. Natl. Acad. Sci. USA *88*, 3382–3386.

Winzeler, E.A., Shoemaker, D.D., Astromoff, A., Liang, H., Anderson, K., Andre, B., Bangham, R., Benito, R., Boeke, J.D., Bussey, H., et al. (1999). Functional characterization of the S. cerevisiae genome by gene deletion and parallel analysis. Science *285*, 901–906.

World Health Organization (2014). World Malaria Report. http://www.who.int/malaria/publications/world_malaria_report_2014/en/.

STAR★METHODS

KEY RESOURCES TABLE

REAGENT or RESOURCE	SOURCE	IDENTIFIER
Antibodies		
Mouse monoclonal anti-SAG1 (clone DG52)	(Burg et al., 1988)	N/A
Mouse monoclonal anti-TUB1 (clone 12G10)	Developmental Studies Hybridoma Bank at the University of Iowa	RRID: AB_1157911
Mouse monoclonal anti-MIC2 (clone 6D10)	(Achbarou et al., 1991)	N/A
Mouse monoclonal anti-Ty1 (clone BB2)	(Bastin et al., 1996)	N/A
Mouse monoclonal anti-FLAG (clone M2)	Sigma-Aldrich	Cat#F3165
Mouse monoclonal anti-HA (clone 16B12)	BioLegend	Cat#901501
Alpaca nanobody anti-CDPK1(clone 1B7)	(Ingram et al., 2015)	N/A
Rabbit polyclonal anti-MyoA	(Frénal et al., 2014)	N/A
Rabbit polyclonal anti-PLP1	(Kafsack et al., 2009)	N/A
Rabbit polyclonal anti-ACT1	(Dobrowolski et al., 1997)	N/A
Goat anti-Mouse IgG (H+L) Secondary Antibody, DyLight 488 conjugate	Thermo Fisher	Cat#35502
Goat anti-Rabbit IgG (H+L) Secondary Antibody, DyLight 594 conjugate	Thermo Fisher	Cat#35560
Pacific Blue Antibody Labeling Kit	Thermo Fisher	Cat#P30013
Alexa Fluor 594 Antibody Labeling Kit	Thermo Fisher	Cat#A20185
Chemicals, Peptides, and Recombinant Proteins		
Pyrimethamine	Sigma-Aldrich	Cat#46706
Mycophenolic Acid	Sigma-Aldrich	Cat#M3536
Xanthine	Sigma-Aldrich	Cat#X4002
Gentamicin	Thermo Fisher	Cat#15710072
5-Fluoro-2′-deoxyuridine (FUDR)	Sigma-Aldrich	Cat#F0503
Rapamycin	EMD Millipore	Cat#553210
A23187	EMD Millipore	Cat#100105
Zaprinast	EMD Millipore	Cat#684500
Blasticidin S	Sigma-Aldrich	Cat#15205
WR99210	Sigma Aldrich	Cat#W1770
Anhydrotetracycline	Takara-Clontech	Cat#631310
SYBR Green I	Thermo Fisher	Cat#S7563
Ampicillin	Sigma-Aldrich	Cat#A0166
Critical Commercial Assays		
QuikChange Multi-Site Directed Mutagenesis Kit	Agilent Technologies	Cat#200514
Gibson Assembly Cloning Kit	New England Biolabs	Cat#E5510S
NucleoBond Xtra Midi	Macherey Nagel	Cat#740412.50
DNeasy Blood & Tissue Kit	QIAGEN	Cat#69506
RNeasy Plus Kit	QIAGEN	Cat#73404
ProtoScript First Strand cDNA Synthesis Kit	New England Biolabs	Cat#E6300S
Surveyor Mutation Detection Kit	Integrated DNA Technologies	Cat#706020
Deposited Data		
T. gondii strain GT1 genome, release 28	ToxoDB	http://toxodb.org/toxo/
Ortholog Groups of Protein Sequences, version 5	OrthoMCL DB	http://orthomcl.org/orthomcl/

(*Continued on next page*)

Continued

REAGENT or RESOURCE	SOURCE	IDENTIFIER
Experimental Models: Cell Lines		
Human Foreskin Fibroblasts (HFFs)	ATCC	SCRC-1041
Human Erythrocytes	Research Blood Components, LLC	N/A
Experimental Models: Organisms/Strains		
T. gondii: strain RH	ATCC	50838
T. gondii: strain RH/Cas9	This paper	N/A
T. gondii: strain RH/Δ*KU80*/Δ*HXGPRT*	ATCC	PRA-319
T. gondii: strain RH/Δ*KU80*/Δ*RAB4*	This paper	N/A
T. gondii: strain TATi/Δ*KU80*	(Sheiner et al., 2011)	N/A
T. gondii: strain RH/Cas9/H2B-YFP	This paper	N/A
T. gondii: strain DiCre/Δ*KU80*/KillerRed$_{flox}$-YFP	(Pieperhoff et al., 2015)	N/A
T. gondii: strain DiCre/CLAMP cKD	This paper	N/A
P. falciparum: strain NF54$_{attB}$	Laboratory of David A. Fidock	N/A
P. falciparum: strain *Pf*CLAMP cKD	This paper	N/A
Recombinant DNA		
pU6-Universal	Addgene	Cat#52694
pCas9/decoy	This paper	N/A
pH2B-YFP/decoy	This paper	N/A
pU6-DHFR	This paper; Addgene	Cat#80329
pLIC-HA-FLAG-(3′UTR$_{SAG1}$-pDHFR-HXGPRT-5′UTR$_{DHFR}$)$_{flox}$-4xU1	(Pieperhoff et al., 2015)	N/A
pPfCLAMP-cKD/TetR-DOZI	(Ganesan et al., 2016)	N/A
pU6[sgSAG1]-DHFR	This paper; Addgene	Cat#80322
pU6-Decoy	This paper; Addgene	Cat#80324
pCas9/CAT	This paper; Addgene	Cat#80323
Genome-wide sgRNA library	Addgene	Cat#80636
Sequence-Based Reagents		
All primers and oligonucleotides are listed in Table S2	This paper	N/A
Software and Algorithms		
ClustalW	(Larkin et al., 2007)	http://www.clustal.org/clustal2/
Bioperl, version 1.5.2	BioPerl	http://bioperl.org/
R, version 3.2.3	R Foundation for Statistical Computing	https://www.R-project.org/
Prism, version 6.0	GraphPad	http://www.graphpad.com
FIJI running ImageJ, version 2.0	(Schindelin et al., 2012)	http://imagej.net/Welcome
sgRNA library design scripts	(Wang et al., 2014)	N/A
Screen analysis scripts	This paper	N/A
Other		
Genome-wide screening data	This paper	Table S3

CONTACT FOR REAGENT AND RESOURCE SHARING

Further information and requests for reagents may be directed to, and will be fulfilled by the corresponding author Sebastian Lourido (lourido@wi.mit.edu).

EXPERIMENTAL MODEL AND SUBJECT DETAILS

T. gondii tachyzoites from the strain RH and derived strains were maintained at 37°C with 5% CO_2 growing in human foreskin fibroblasts (HFFs) cultured in DMEM supplemented with 10% heat-inactivated fetal bovine serum and 10 μg/ml gentamicin. When appropriate, chloramphenicol was used at 40 μM and pyrimethamine at 3 μM (1.5 μM for plaque assays).

P. falciparum parasites of the strain NF54^{attB} (kindly provided by David Fidock) and the derived strain were grown in human erythrocytes (Research Blood Components) at 5% hematocrit under 5% O_2 and 5% CO_2 in RPMI 1640 media supplemented with 5 mg/ml Albumax II (Life Technologies), 2 mg/ml $NaHCO_3$, 25 mM HEPES (pH 7.4), 1 mM hypoxanthine and 50 μg/ml gentamicin.

METHOD DETAILS

Plasmid Design and Construction

To construct pCas9/CAT, the chloramphenicol acetyltransferase (CAT) gene, under the *TUB1* promoter and *SAG1* 3′ UTR (Soldati and Boothroyd, 1993), was amplified using primers P1 and P2 (see Table S2 for a complete list of primers and oligonucleotides), and ligated into the PciI and XbaI sites of pU6-Universal (Addgene, #52694). To generate pCas9/decoy, oligonucleotides P3 and P4 were hybridized and cloned into the BsaI sites of pU6-Universal. H2B-YFP (Hu et al., 2004) was excised with NsiI and NotI, and used to replace Cas9 in pCas9/decoy by ligating the fragment into the same restriction sites to generate pH2B-YFP/decoy.

The plasmid for sgRNA expression was constructed by amplifying the pyrimethamine-resistance cassette (Donald and Roos, 1993) with primers P5 and P6, and cloning it into the NsiI and SbfI sites of pU6-Universal. Three BsaI sites in DHFR were eliminated using the QuikChange multi-site directed mutagenesis kit (Agilent Technologies) with primers P7, P8, and P9 resulting in the plasmid pU6-DHFR. The SAG1 protospacer, encoded by primers P10 and P11, was cloned into pU6-DHFR as described above for the decoy protospacer. Guides for gene disruption (P14–P63) and ICAP tagging (P80–P113) were synthesized for Gibson Assembly (New England Biolabs) into pU6-DHFR or pU6-Universal, respectively. Such guides and their reverse complements were hybridized, and Gibson cloned into their respective vectors linearized with BsaI. Guides to knock out *RAB4* were similarly generated by cloning sgRNAs against the 5′ (P160 and P161) and 3′ (P162 and P163) ends of the coding sequence into pU6-Universal.

For C-terminal HA-FLAG epitope tagging and U1 mediated knockdown, a 3′ flank of the *CLAMP* gene, upstream of the stop codon, was amplified by PCR with primers P148 and P149 and inserted into pLIC-HA-FLAG-(3′UTR$_{SAG1}$-pDHFR-HXGPRT-5′UTR$_{DHFR}$)$_{flox}$-4xU1 (Pieperhoff et al., 2015) by ligation-independent cloning (Huynh and Carruthers, 2009) to generate pCLAMP-U1.

The plasmid for conditional knockdown of CLAMP in *P. falciparum* was generated by amplifying the 5′ and 3′ homology regions from the CLAMP locus using primers P152–P155. P155 included an sgRNA targeting the 3′ end of the CLAMP locus, placed under the regulation of the T7 promoter in the final construct. The fragments were cloned by Gibson assembly into the plasmid containing the aptamers, and the *Renilla* luciferase-blasticidin deaminase fusion separated from the TetR-DOZI fusion by a T2A self-cleaving peptide, to generate p*Pf*CLAMP-cKD/TetR-DOZI (Ganesan et al., 2016).

Library Design and Construction

Ten guides were designed against each gene in the 14 annotated chromosomes of the *T. gondii* GT1 genome (release 28, ToxoDB.org), according to published guidelines (Wang et al., 2014). Briefly, selection of sgRNAs was weighted based on targeting of exons, number of potential off-target sequences, and overlap between sgRNAs for a given gene. A ‘G’ was prepended to any sgRNAs that did not start with one to ensure proper RNA polymerase III initiation. Guides against *DHFR* and *HXGPRT* were removed from the library to preclude interference with drug-resistance markers. The guide library was synthesized by CustomArray, and includes guides flanked by sequences for Gibson Assembly into pU6-DHFR. The sgRNA library was amplified using primers P12 and P13, and Gibson cloned into pU6-DHFR linearized with BsaI. Assembled constructs were transformed into Mega-X DH10B electrocompetent *Escherichia coli* (Life Technologies), allowed to recover for 1 hr, and grown overnight with 100 μg/ml ampicillin, prior to large-scale plasmid isolation (Macherey Nagel) or frozen storage. Cloning and electroporation efficiencies were monitored to ensure proper library coverage.

T. gondii Strain Generation

All transfections were performed as described previously with a square-wave electroporator (Sidik et al., 2014). RH/Cas9 and RH/Cas9/H2B-YFP were generated by co-transfecting RH with 50 μg each of pCas9/CAT and pCas9/decoy, or pH2B-YFP/decoy and pCas9/CAT, respectively. Stable transgenic strains were selected with 40 μM chloramphenicol. Single clones were isolated by limiting dilution and screened for the presence of Cas9 using immunofluorescence and immunoblotting against the triple-FLAG tag. The decoy protospacer was amplified by PCR from RH/Cas9 genomic DNA using primers P64 and P65, and confirmed by sequencing.

To generate the *RAB4* knockout, the pyrimethamine-resistance cassette was amplified from pU6-DHFR with primers P164 and P165 to contain homology regions to replace the entire open reading frame. The amplicon was cotransfected along with two pU6-Universal plasmids carrying guides against the 5′ and 3′ end of the coding sequence into RH/Δ*KU80* parasites (Huynh and Carruthers, 2009). Stable transformants were selected for with pyrimethamine and clones were isolated by limiting dilution. Correct integration of the pyrimethamine-resistance cassette into the *RAB4* locus was confirmed using P166 and P169 to amplify the 5′ junction, and P167 and P168 to amplify 3′ junction. Deletion of the *RAB4* locus was assessed using P170 and P171 to amplify a portion of the open reading frame. Fitness of the *RAB4* knockout was determined by plaque assay, as described below.

To generate the CLAMP conditional knockdown (DiCre/CLAMP), 25 μg of pCLAMP-U1 were linearized with MfeI for efficient homologous recombination and transfected into DiCre/Δ*ku80*/*KillerRed$_{flox}$-YFP* (DiCre) (Pieperhoff et al., 2015). Following selection with 25 μg/ml mycophenolic acid and 50 μg/ml xanthine, individual clones were obtained by limiting dilution.

Pooled CRISPR Screens

For each biological replicate, 400 μg of the sgRNA library were linearized with AseI, dialyzed against water, and transfected into approximately 4 × 10^8 RH or RH/Cas9 parasites divided between 8 separate cuvettes. Transfections were used to infect 8 T-175 flasks with confluent HFF monolayers, and pyrimethamine was added 24 hr later. The parasites were allowed to egress naturally from host cells two days after infection, isolated by filtration, and 1.5 × 10^8 parasites were passaged onto 8 T-175 flasks with fresh monolayers. The remaining parasites (~10^7) were pelleted and stored at −80°C for analysis. This process was repeated again 5 days and 7 days post-transfection. For the drug-resistance screens, 5 μM 5-fluorodeoxyuridine (FUDR; Sigma) was added to 1.2 × 10^7 parasites collected on day 7 post transfection, and parasites were cultured until their first lysis. Untreated mutant pools were maintained in parallel for the duration of FUDR selection. Parasite DNA was extracted using the DNeasy Blood and Tissue kit (QIAGEN) and integrated sgRNA constructs were amplified using a nested PCR with primers P74 and P75 followed by P76 and P77. The resulting libraries were sequenced on a HiSeq 2500 (Illumina) with single-end reads using primers P150 and P151.

RT-PCR

RAB4 expression was assessed in both the parental and Δ*RAB4* strains by RT-PCR. Total RNA was prepared from isolated parasites using the RNeasy Plus Kit (QIAGEN). The ProtoScript First Strand cDNA Synthesis Kit (New England Biolabs) was used to prepare cDNA, and reverse transcriptase (RT) was excluded from the control reactions. PCR was performed on the cDNA samples with primers specific for *RAB4* (P174 and P175) or the *ACT1* control (P172 and P173).

Functional Analysis of ICAPs and Controls

1.25 × 10^7 RH/Cas9 or RH/Cas9/H2B-YFP parasites were transfected with 50–100 μg of pU6-DHFR containing guides against different ICAPs or controls. If aiming for integration, plasmids were linearized with AseI and dialyzed against water prior to transfection. Transfected parasites were seeded on HFFs at a MOI of 10, and pyrimethamine was added 24 hr after transfection. Parasites transected with sgSAG1 were allowed to egress from host cells two days after transfection, and used to infect host cells seeded on coverslips. SAG1 loss was quantified by immunofluorescence 24 hr after infecting coverslips, which was equivalent to three days after transfection.

To screen for ICAPs that participate in invasion, parasites were released from host cells 24 hr after transfection by passage through a 27.5-gauge needle, and used to infect fresh monolayers, thus extending the time allowed for protein depletion. To test invasion, freshly lysed parasites were suspended in invasion media (DMEM supplemented with 1% FBS, 20 mM HEPES [pH 7.4]). 2 × 10^5 parasites per well were added to confluent HFF monolayers grown in 96-well plates and centrifuged at 290 × *g* for 5 min. Invasion was allowed to proceed for 10 min at 37°C, before the monolayers were fixed in 4% formaldehyde for 20 min on ice. Extracellular parasites were stained using mouse-anti-SAG1 (Burg et al., 1988) conjugated to Alexa-Fluor-594 (Life Technologies), and host cell nuclei were stained using Hoechst (Santa Cruz). Images were acquired using a Cytation 3 imager (BioTek), and analyzed using custom FIJI (Schindelin et al., 2012) macros to count the number of parasites and host-cell nuclei.

ICAP Tagging

CRISPR-mediated C-terminal Ty tagging was performed as previously described (Sidik et al., 2014). 30 μg of a repair oligonucleotide containing an in-frame Ty epitope (Bastin et al., 1996) flanked by homology regions to the C terminus of each gene (P114–P147) were co-transfected with 100 μg of pU6-Universal carrying the appropriate sgRNA into TATi/Δ*KU80* parasites (Sheiner et al., 2011). Transfected parasites were cultured until their first lysis and used to infect confluent HFF monolayers grown on coverslips. Localization of the Ty-tagged ICAPs was determined 24 post infection by immunofluorescence microscopy.

C-terminal tagging of CLAMP with mNeonGreen, was accomplished by amplifying the fluorescent protein coding sequence with primers P78 and P79 from a template plasmid (kindly provided by Ke Hu). 30 μg of the resulting product were co-transfected into TATi/Δ*KU80* parasites along with 100 μg of pU6-Universal carrying an sgRNA against the C-terminal sequence of the endogenous CLAMP locus. Fluorescent parasites were isolated by FACS two days post transfection, and cloned by limiting dilution. Correct integration of mNeonGreen into the CLAMP locus was confirmed by sequencing.

CLAMP Phylogeny and Topology Predictions

CLAMP homologs were readily identified by BLAST searches against all sequenced apicomplexan genomes (EupathDB.org). Sequences were curated for *Babesia* and *Theileria* spp. to correct errors in the gene models. Alignment was performed using ClustalW (Larkin et al., 2007) and the phylogenetic tree was generated by neighbor-joining excluding positions with gaps. Bootstrap values were calculated for 10,000 trials. A hidden Markov model-based search was performed for the alignment using HHpred (Meier and Söding, 2015). Significant structural similarity was found between CLAMP and Claudin-19 ($p = 4.1 \times 10^{-9}$), Claudin-15 ($p = 7.3 \times 10^{-9}$), and the voltage-gated calcium channel γ subunit 15 ($p = 10^{-10}$), which all belong to the same tetraspan family (Simske, 2013). Structural similarity between CLAMP and Claudin-19 (95% confidence) was also found using Phyre2 (Kelley et al., 2015). Topology prediction was performed against several representative orthologs with CCTOP (Dobson et al., 2015) and in all cases arrived at the same prediction of four transmembrane domains with cytoplasmic N and C termini (Figure S4).

CLAMP Conditional Knockdown

DiCre/CLAMP parasites were treated with 50 nM rapamycin or vehicle control for 2 hr, then cultured for 48 hr before phenotypic analysis by immunoblot, plaque formation, MIC2 secretion, or invasion assay.

Immunofluorescence Microscopy and Immunoblotting

Mouse monoclonal antibodies were used to detect SAG1 (clone DG52; Burg et al., 1988), TUB1 (clone 12G10, Developmental Studies Hybridoma Bank at the University of Iowa), MIC2 (clone 6D10; Achbarou et al., 1991), Ty-tagged proteins (clone BB2; Bastin et al., 1996), FLAG-tagged proteins (clone M2; Sigma-Aldrich), and HA-tagged proteins (clone 16B12; BioLegend). CDPK1 was detected using the alpaca-derived nanobody 1B7 (Ingram et al., 2015). Rabbit polyclonal sera were used to detect MyoA (Frénal et al., 2014), PLP1 (Kafsack et al., 2009) and ACT1 (Dobrowolski et al., 1997).

Prior to immunoblotting, DiCre and DiCre/CLAMP parasites were suspended in lysis buffer (137 mM NaCl, 10 mM $MgCl_2$, 1% Triton X-100, Halt protease inhibitors [Thermo Fisher], 20 mM HEPES [pH 7.5]). An equal volume of 2X Laemmli buffer (4% SDS, 20% glycerol, 5% β-mercaptoethanol, 0.02% bromophenol blue, 120 mM Tris-HCl [pH 6.8]) was added, and the samples were heated to 37°C for 10 min prior to separation of proteins by SDS-PAGE. After transferring separated proteins to nitrocellulose, the membrane was incubated in stripping buffer (100 mM β-mercaptoethanol, 2% SDS, 62.5 mM Tris-HCl [pH 6.8]) for 15 min at 50°C, then washed twice in TBS-T (20 mM Tris-HCl, 138 mM NaCl, 0.1% Tween-20 [pH 7.5]). Samples for all other blots were prepared similarly, but boiled 10 min prior to separation by SDS-PAGE, and membranes were not incubated in stripping buffer. β-mercaptoethanol was not included when probing for SAG1.

Intracellular parasites were fixed with either methanol at 4°C for 2 min, or 4% formaldehyde for 10 min. Staining was performed with the antibodies described above and detected with Alexa-Fluor-labeled secondary antibodies. Formaldehyde-fixed samples were permeablized with 0.25% Triton X-100 in PBS for 8 min. Nuclei were stained with Hoechst (Santa Cruz) or DAPI (Life Technologies) and coverslips were mounted in Prolong Diamond (Thermo Fisher). Images were acquired using an Eclipse Ti epifluorescence microscope (Nikon) using the NIS elements imaging software. FIJI was used for image analysis, and Adobe Photoshop for image processing.

Surveyor Assays

Pools of mutant parasites were suspended in PBS containing 200 μg/ml Proteinase K (Sigma-Aldrich) and 1X Taq PCR Buffer (Sigma-Aldrich) and heated to 37°C for 1 hr, 50°C for 2 hr, and 95°C for 15 min. Mutated regions were then amplified using primers for the *SAG1* locus (P66 and P67), the *MyoA* locus (P68 and P69), the *PLP1* locus (P70 and P71) or the *CDPK1* locus (P72 and P73). Surveyor reactions were performed using a kit according to the manufacturer's instructions (Integrated DNA Technologies).

Plaque Formation

4×10^6 RH/Cas9/H2B-YFP parasites were transfected with 50 μg of pU6-DHFR encoding guides against ICAPs or controls. 2,000 transfected parasites were added to HFF monolayers in 6-well plates. 1.5 μM pyrimethamine was added one day post-transfection. Ten days post transfection, the monolayers were rinsed with PBS, fixed in 95% ethanol for 10 min and stained with crystal violet (2% crystal violet, 0.8% ammonium oxalate, 20% ethanol) for 5 min. 500 parasites per well were used to analyze the effect of CLAMP or RAB4 on plaque formation over the course of 8 days.

Microneme Secretion

Microneme secretion assays were performed as previously described (Lourido et al., 2012). 2×10^7 DiCre or DiCre/CLAMP parasites were suspended in DMEM, then treated with 3% FBS with or without 1% ethanol for 10 min at 37°C, 5% CO_2. Supernatants were collected by centrifugation 10 min at 400 *g*, 4°C. Proteins were separated by SDS-PAGE, and secreted MIC2 was quantified and normalized to MIC2 levels in total lysates measured by immunoblotting.

Egress Assays

4×10^6 DiCre or DiCre/CLAMP parasites were treated with 50 nM rapamycin or vehicle upon infection of HFF monolayers in 96-well plates. Rapamycin was removed after two hours, and parasites were allowed to grow for 24–30 hr. Egress was induced with 1 μM A23187 (EMD Millipore) for 10 min. Knockdown parasites in the rapamycin-treated samples were identified by expression of the YFP reporter. The number of intact vacuoles before or after the induction of egress was quantified. Only YFP-expressing vacuoles were counted for the rapamycin-treated samples.

Invasion Assays

DiCre and DiCre/CLAMP parasites were suspended in invasion media and 5×10^6 parasites were added per well of a 24-well plate containing HFF monolayers seeded on coverslips. Invasion was allowed to proceed at 37°C with 5% CO_2 for 20 min. HFF cells and parasites were fixed with 4% formaldehyde for 20 min on ice. Extracellular parasites were stained with Pacific Blue-conjugated anti-SAG1 prior to permeabilization, and all parasites were stained with Alexa-Fluor-594-conjugated anti-SAG1 after permeabilization with 0.25% Triton. The average number of host cells per field of view was obtained from coverslips prepared and processed in parallel and stained with Hoechst. The number of invaded parasites per fields were manually counted and normalized to the number of

host cells in the same area. CLAMP-mNeonGreen parasites were prepared similarly and allowed to invade for 30 min before being fixed with 4% formaldehyde for 20 min on ice. Extracellular parasites were stained with Alexa-Fluor-594-conjugated anti-SAG1.

Video Microscopy

To capture egress, DiCre or DiCre/CLAMP parasites were prepared as described for the egress assays in glass-bottom 35 mm dishes (MatTek). Parasites were stimulated to egress with 1 μM A23187 or 500 μM zaprinast, and recorded at 2–5 frames per second for ten minutes, using an Eclipse Ti microscope (Nikon) with an enclosure heated to 37°C. The same setup was used to capture invasion, with the exception that freshly lysed parasites were added directly to monolayers under observation.

P. falciparum Strain Generation and Analysis

The *P. falciparum* NF54^{attB} strain (kindly provided by David Fidock) was modified to generate a strain NF54$^{Cas9+T7\ Polymerase}$, which contained Cas9 and T7 RNA polymerase expression cassettes integrated into the attB site. Linearized p*Pf*CLAMP-cKD/TetR-DOZI was transfected into NF54$^{Cas9+T7\ Polymerase}$. 50 μg of plasmid were used per 200 μl packed red blood cells (RBCs), adjusted to 50% hematocrit, and electroporated as previously described (Ganesan et al., 2016). Transfected parasites were selected with a combination of 2.5 μg/ml Blasticidin S and 2.5 nM WR99210 beginning 4 days after transfection. The *Pf*CLAMP cKD strain was maintained in 0.5 μM anhydrotetracycline (aTc). Correct integration of the construct was confirmed by PCR and sequencing using primer pairs P156/P157 and P158/P159.

To analyze *P. falciparum* growth upon CLAMP downregulation, parasites were synchronized to rings using 0.5 M alanine in 10 mM HEPES (pH 7.4), adjusted to 1% parasitemia, and seeded in triplicate wells of a 12-well plate at 2% hematocrit in 5 ml of media with or without aTc. The parental and *Pf*CLAMP cKD strains were treated in parallel. Expansion was measured over six lytic cycles. Samples were collected after each cycle to measure parasitemia by incubating the cells with a 1:5000 dilution of SYBR Green I (Thermo Fisher) for 15 min at 37°C, prior to flow-cytometry on an Accuri C6 instrument (BD Biosciences). Following the analysis, all cultures were subcultured using the same dilution factor, as required to maintain the pre-invasion parasitemia of the parental lines at 1%, and avoid over-expansion of the cultures. After subculturing, the pre-invasion parasitemia was directly measured as indicated above. Parasite growth was expressed as percent parasitemia at the start and end of each lytic cycle.

QUANTIFICATION AND STATISTICAL ANALYSIS

Bioinformatic Analysis of the Screening Results

Sequencing reads were aligned to the sgRNA library. The abundance of each sgRNA was calculated and normalized to the total number of aligned reads. Guides that were not found were assigned a pseudo-count corresponding to 90% of the lowest value in that sample. Only guides whose abundance was above the 5th percentile in the original plasmid preparation of the sgRNA library were taken into account for subsequent analyses. For FUDR selection experiments, the $\log_2$ fold change between treated and untreated samples was calculated for each sgRNA, whereas negative selection experiments used the plasmid preparation for comparison. The "phenotype" score for each gene was calculated as the mean $\log_2$ fold change for the top five scoring guides, which minimized the effect of stochastic losses and decreased the error between biological replicates. The mean phenotype score for each gene in four replicates of the screen is reported. Fitness-conferring genes were identified by comparison to 40 control genes known to be dispensable for parasite growth in fibroblast (see Table S1). For a given gene, the four biological replicates were compared to the mean phenotype of the controls using a one-sided t test, and the $\log_2$ fold changes for the sgRNAs against that gene were compared to the sgRNAs against the controls using a one-sided Mann-Whitney *U* test. The *p* values for each test were corrected using the Benjamini-Hochberg method. Genes were considered fitness-conferring if they met a significance threshold of 0.05 for both tests. 10-fold cross-validation was performed using the set of previously described essential and dispensable genes (Table S1). In each trial, the test sample was compared using the statistical tests described to the control genes in the training set. The cross-validation was performed 100 times to estimate the error rate.

Gene-set enrichment analysis was performed as previously described (Subramanian et al., 2005), using gene sets specifically curated for *T. gondii* (Croken et al., 2014). Gene expression data (kindly provided by David S. Roos and Maria Alejandra Diaz-Miranda, available through ToxoDB) consisted of RNA samples collected at several time points following infection with *T. gondii* strain GT1 tachyzoites, and analyzed by RNaseq. The maximum $\log_2$(RPKM + 1) was used for the analysis and compared to the mean phenotype score for each gene. To compare the phenotype scores with the rate of evolution, syntenic orthologs that did not display copy-number variation were obtained from ToxoDB release 26 for *T. gondii* GT1, *Neospora caninum* Liverpool, and *Hammondia hammondi* HH34. d_N/d_S ratios were determined as previously described (Lorenzi et al., 2016). Briefly, average d_N/d_S values were calculated according to Goldman & Yang (Goldman and Yang, 1994), following alignment of cDNA sequences based on their protein sequence by ClustalW (Larkin et al., 2007). The distribution of phenotype scores in the top and bottom third of the d_N/d_S distribution were compared by a Kolmogorov-Smirnov test. Depth of conservation of *T. gondii* genes was estimated using ortholog groupings of 79 eukaryotic genomes available through OrthoMCL DB release 5 (Chen et al., 2006). Assignment to the different levels of conservation was performed by asking whether an ortholog was present in at least one of the genomes from a neighboring branch. For simplicity, genes that did not conform to a simple assignment were excluded from this analysis (Other) and specific losses in either hematozoa (piroplasmida and *Plasmodium* spp.) or cryptosporidia were allowed when assigning a gene to the apicomplexan category.

Statistical Testing

The ratio of plaquing efficiency following mutation of each ICAP relative to SAG1 mutation was compared to a mean of 1 using one-tailed t tests, and the resulting *p* values were corrected using the Benjamini-Hochberg method. Based on the small sample size, mutants with a corrected *p* value lower than 0.1 were considered significant. ICAP mutant invasion efficiency was analyzed similarly using PLP1 as the control. The effects of inducing CLAMP knockdown on invasion, egress, and MIC2 secretion were analyzed in Prism (GraphPad) using two-tailed t tests with a *p* value of 0.05 or lower indicating significance. Where appropriate, statistical parameters including the exact value of *n*, the definition of center, dispersion, and precision measures and statistical significance are reported in the figures and corresponding legends.

DATA AND SOFTWARE AVAILABILITY

Software

Guide selection and screen analysis were performed using custom software that will be provided upon request. Statistical analyses were performed in R (http://www.R-project.org) using built-in packages unless otherwise indicated.

Data Resources

All data from the CRISPR screens is available in Table S3, and will be integrated into an upcoming release of ToxoDB (http://ToxoDB.org).

Cell

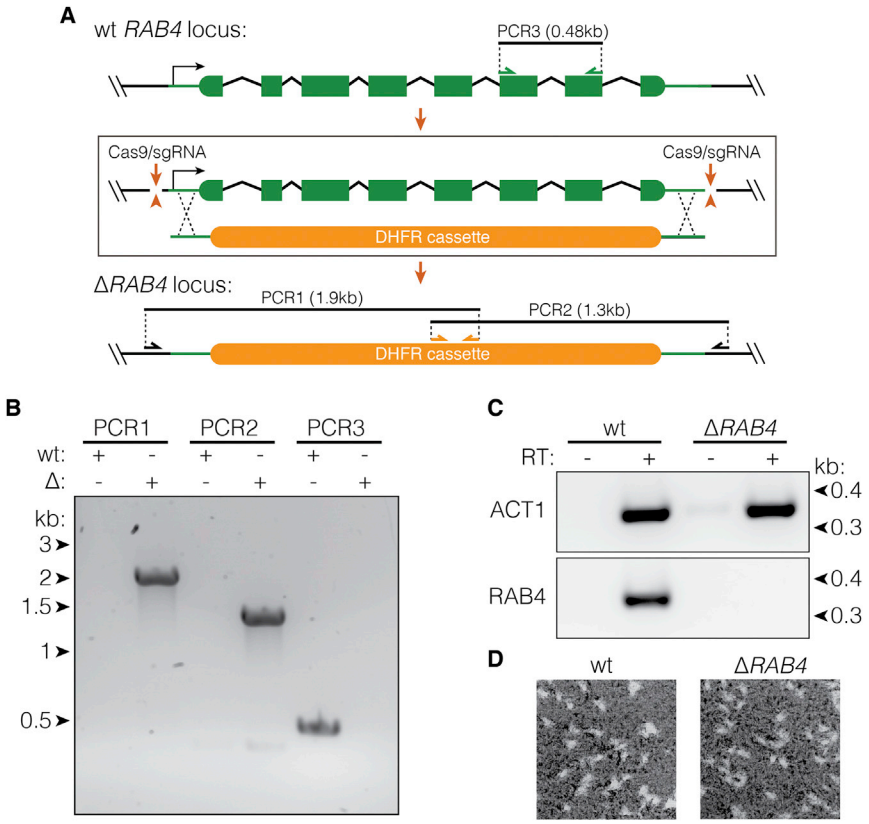

Figure S1. RAB4 Is Not Essential for *T. gondii* Growth in Human Fibroblasts, Related to Figure 3

(A) Diagram of the *RAB4* locus illustrating the knockout strategy and position of the primers used for validation. Specific primers were used to amplify the 5′ (PCR1) and 3′ (PCR2) junctions, and a segment of the coding sequence (PCR3).

(B) PCR assay for integration of the pyrimethamine-resistance cassette into the *RAB4* locus and deletion of the *RAB4* coding sequence.

(C) RT-PCR probing for expression of RAB4 or the control ACT1 on cDNA samples prepared with or without reverse transcriptase (RT).

(D) Plaque assay demonstrating normal growth of the *RAB4* knockout in human fibroblasts.

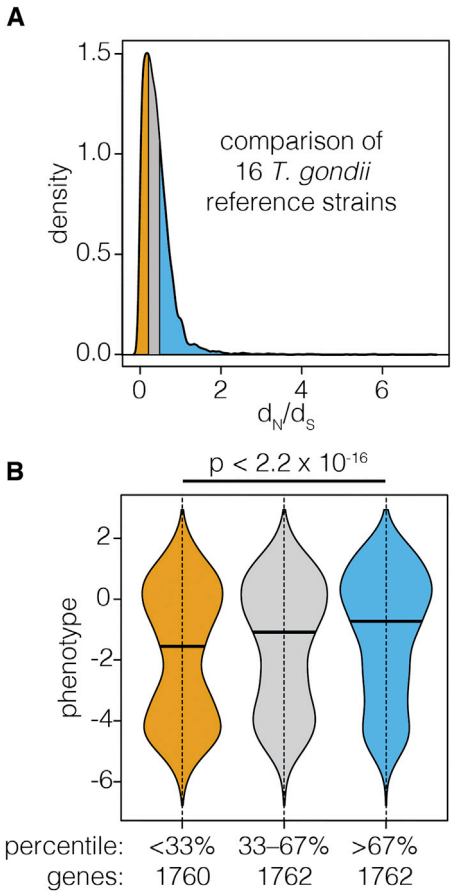

Figure S2. Correlation of Phenotype Scores to Selective Pressure, Related to Figure 3

(A) Distribution of published d_N/d_S values for 16 reference *T. gondii* genomes (Lorenzi et al., 2016). The lowest and highest third of the dataset is highlighted in orange and blue, respectively.

(B) Genes binned according to d_N/d_S show higher phenotype scores for genes under positive selection (blue), compared to those under negative selection (orange). Bars indicate the group median. The distributions were compared using a Kolmogorov-Smirnov test.

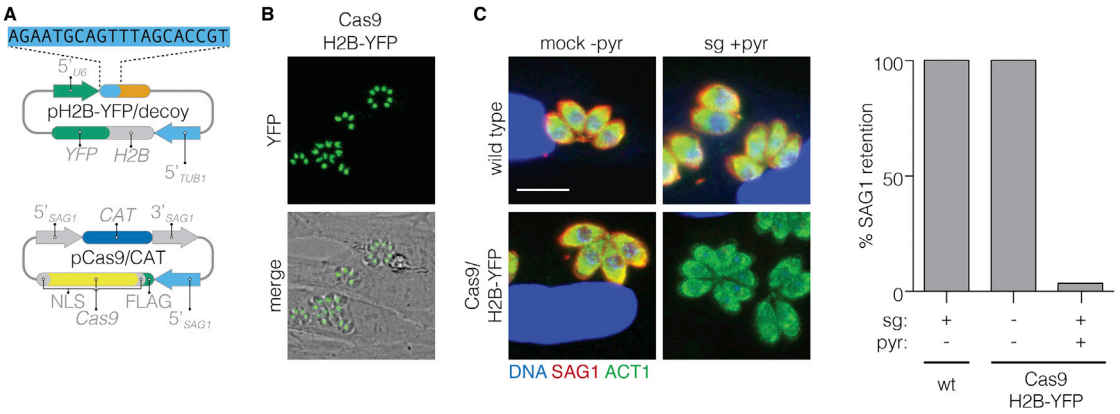

Figure S3. Construction and Validation of the Cas9 Strain Expressing H2B-YFP, Related to Figure 5

(A) Diagram of the constructs used to generate the *T. gondii* strain expressing H2B-YFP and Cas9. The sequence of the decoy sgRNA is highlighted in the top construct, followed by the Cas9-binding sequence (orange).

(B) Expression of H2B-YFP in the nucleus of the clonal parasites detected by live fluorescence video microscopy.

(C) Representative micrographs showing intracellular parasites three days post transfection. Parasites were stained for SAG1 (red), and TgACT1 (ACT; green). Host-cell and parasite nuclei were stained with DAPI (blue). Scale bar, 10 μm. SAG1 retention in wild-type (wt) and Cas9-expressing parasites was measured following the different treatments.

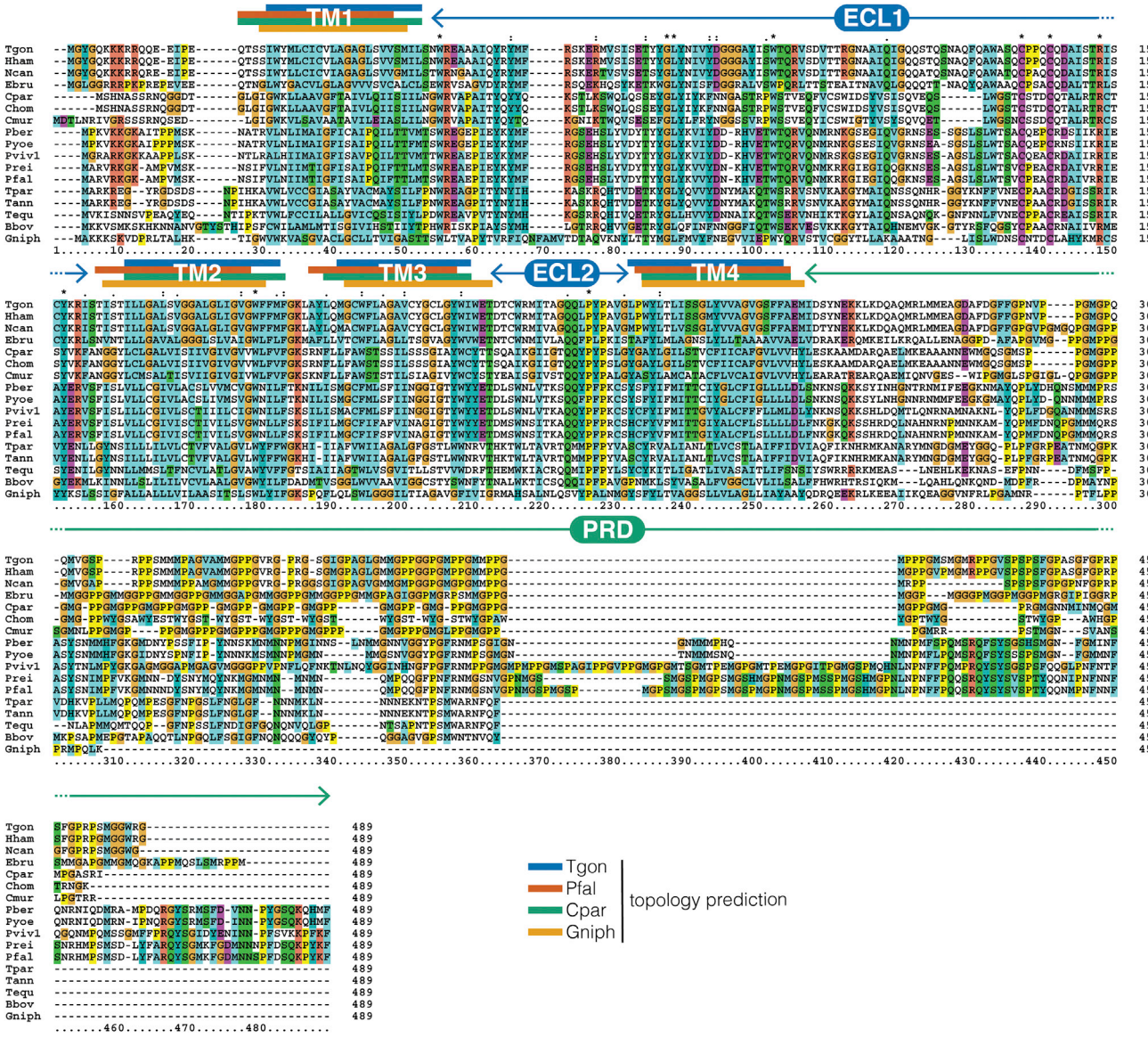

Figure S4. Alignment of CLAMP Orthologs, Related to Figure 6

CLAMP orthologs representing the entire breadth of the apicomplexan radiation were aligned using Clustal X. Bars indicate the topology of four representative sequences determined by CCTOP (Dobson et al., 2015). The predicted transmembrane domains (TMs), extracellular loops (ECLs) and proline-rich domain (PRD) are indicated.

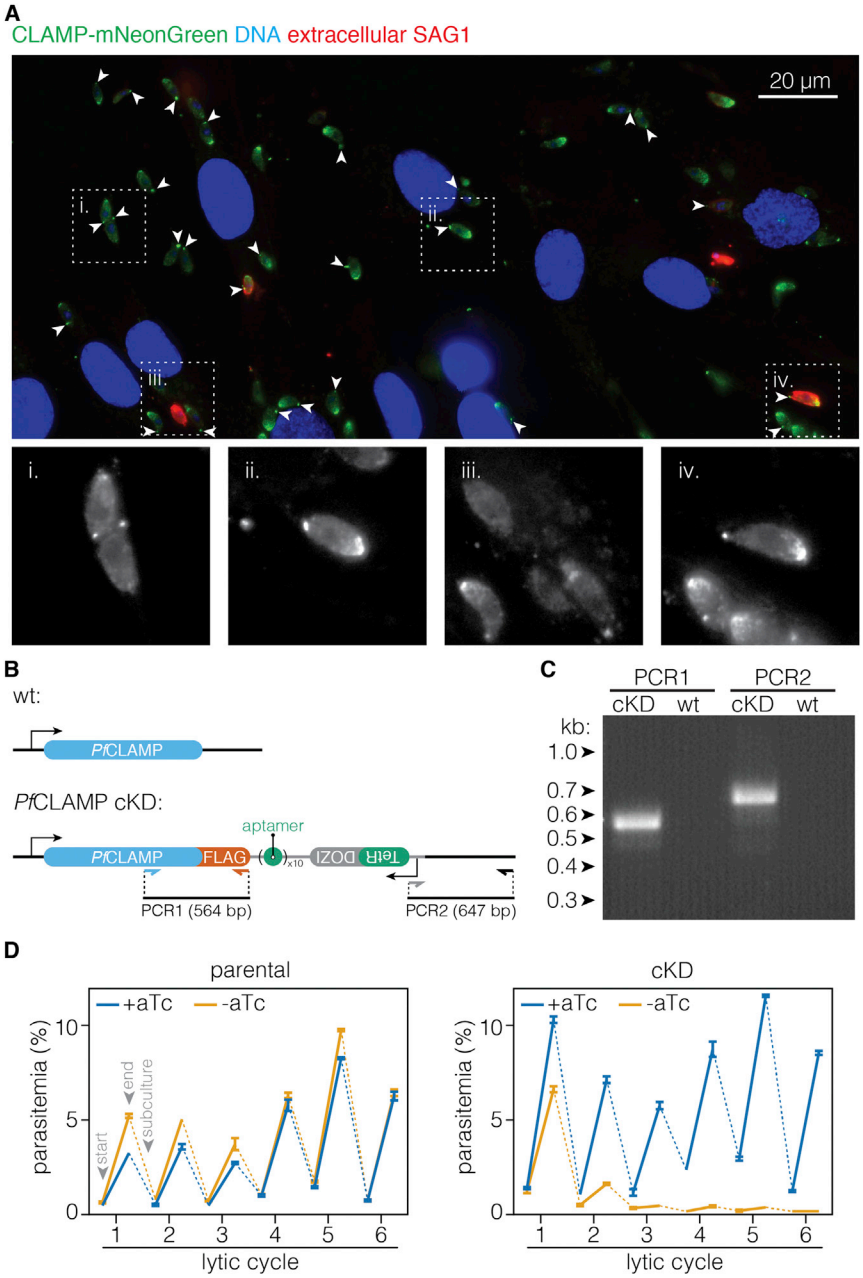

Figure S5. Extended Analysis of CLAMP in *T. gondii* and *P. falciparum*, Related to Figure 6

(A) Localization of CLAMP After Invasion. CLAMP-mNeonGreen parasites were fixed following invasion. Extracellular parasites were stained for the surface antigen SAG1 (red) prior to permeabilization. Arrowheads indicate puncta of mNeonGreen at the posterior of various parasites. Several sections have been magnified to highlight the mNeonGreen localization in invaded (i. and ii.) and non-invaded (iii. and iv.) parasites.

(B and C) Generation and Testing of the *Pf*CLAMP cKD. Diagram of the CLAMP locus for wild-type (wt) and conditional knockdown (cKD) parasites (B). Specific primer pairs (P156/P157 and P158/P159) were used to test for the integration sites (C) and fully sequence them.

(D) Growth curves of the *P. falciparum* parental strain (left) or the cKD (right) ± aTc. Means ± SD for n = 3 technical replicates. This is an independent replicate of the experiment shown in Figure 6N.